

Floquet-engineered diode performance in a Majorana-quantum dot Josephson junction

Koustav Roy,^{1,*} Gourab Paul^{1,†}, Debika Debnath^{1,‡}, Kuntal Bhattacharyya^{1,§} and Saurabh Basu^{1,¶}

¹*Department of Physics, Indian Institute of Technology Guwahati-Guwahati, 781039 Assam, India*

²*Theoretical Physics Division, Physical Research Laboratory, Navrangpura, Ahmedabad-380009, India*

We study nonreciprocal signatures of Josephson current (JC) in a quantum dot (QD)-based Josephson junction (JJ) that comprises of two periodically driven Kitaev chains (KCs) coupled with an intervening QD. The simultaneous breaking of the inversion symmetry (\mathcal{IS}) and the time-reversal symmetry (\mathcal{TRS}), indispensable for the Josephson diode effect (JDE), is achieved solely via the two Floquet drives that differ by a finite phase, which eventually results in a nonreciprocal current, and hence yields a finite JDE. It may be noted that the Floquet Majorana modes generated at both the far ends of the KCs (away from the QD) and adjacent to the QD junctions mediate the JC owing to a finite superconducting (SC) phase difference in the two KCs. We calculate the time-averaged JC and inspect the tunability of the current-phase relation (CPR) to ascertain the diode characteristics. The asymmetric Floquet drive also manifests an anomalous JC signature in our KC-QD-KC JJ. Furthermore, additional control over the QD energy level can be achieved via an external gate voltage that renders flexibility for the Josephson diode (JD) to act as an SC switching device. Tuning different system parameters, such as the chemical potential of the KCs, Floquet frequency, the relative phase mismatch of the drives, and the gate voltage, our model shows the highest possible rectification to be around 70%. Summarizing, our study provides an alternative scenario, replacing the traditional usage of an external magnetic field and spin-orbit coupling effects in a JD via asymmetrically driven Kitaev leads that entail Majorana-mediated transport.

I. INTRODUCTION

Unidirectional current flow in the semiconductor-based p-n junctions [1, 2] has shaped the quantum technologies and device fabrication for decades until the shift in interest to the advent of SC heterojunctions manifesting the direction-dependent dissipationless current [3]. Moreover, the phase difference-induced supercurrent through the SC junctions nowadays is at the forefront of modern condensed matter research due to its nonreciprocal signature which leads to the superconducting diode effect (SDE) [4–13]. In 2018, Tokura and Nagaosa [14] conjectured the possibility of achieving nonreciprocal supercurrent in a noncentrosymmetric crystal through an external magnetic field or magnetochiral anisotropy. The first experimental realization of the SDE by Ando *et al.* [3] in an artificial Rashba superconductor has opened up a compelling avenue for understanding its underlying mechanism based on the principle of simultaneous breaking of the intrinsic symmetries, such as the \mathcal{IS} and the \mathcal{TRS} . Building on their experiment, several theoretical propositions have been put forward in the literature that suggest symmetry breaking through magnetochiral anisotropy [13, 15, 16] or intrinsic magnetic moment [17] that breaks the \mathcal{TRS} . Otherwise, an external magnetic field [3, 12, 18–20] fulfills the requirement.

Experimental realization of the SDE through an intermediate weak link has shown the possibility of con-

trolling the direction of SC current in the JJ [21] which results in an externally controllable Josephson diode effect (JDE) [17, 19, 22–34] with different critical currents in the forward and reverse bias conditions, satisfying $I_c(\phi) \neq -I_c(-\phi)$. Corresponding to a forward bias, the maximum critical current appears as I_c^+ for the SC phase difference $0 \leq \phi \leq \pi$. For the reverse direction, where $\pi \leq \phi \leq 2\pi$ (or $-\pi \leq \phi \leq 0$), the maximum critical current is I_c^- . The sign change in the I_c^+ and I_c^- occurs due to an asymmetric free energy ($E(\phi) \neq E(-\phi)$), which is only possible to achieve via simultaneous breaking of \mathcal{IS} and \mathcal{TRS} . Hence, the finite difference between these two critical JCs $\Delta I_c = I_c^+ - |I_c^-|$ generates nonreciprocity in the JJ, which eventually determines the efficiency of the JJ (controlling the unidirectionality of JC), quantified in the literature through the rectification factor (RF), \mathcal{R} [17, 26, 35, 36] as

$$\mathcal{R} = \left(\frac{\Delta I_c}{I_c^+ + |I_c^-|} \right) \times 100\%. \quad (1)$$

Since the first evidence [3] of SDE, numerous studies have proposed the JDE across a wide range of systems which includes Rashba superconductors [3, 16], van der Waals heterostructures [37], topological insulators [13], Dirac semimetals [38, 39], altermagnets [10, 40] etc. The JDE has also been observed in systems such as a single magnetic atom [18, 41], carbon nanotube [42], InSb nanoflag [43], normal metals [44], and band-asymmetric metals [45]. Additionally, topological superconductors [36, 46] have promised potential applicability as a JDE, highlighting its versatility spanning over different classes of materials.

In particular, recent reports on the JDE have garnered the role of a QD [47–49] that exhibits a single quantized energy level, and can act as a quantum point contact as

* koustav.roy@iitg.ac.in

† p.gourab@iitg.ac.in

‡ debika@prl.res.in

§ kuntalphy@iitg.ac.in

¶ saurabh@iitg.ac.in

the simplest prototype of a weak link for a JJ setup [17–19, 31, 41, 50]. In addition to its fundamental interest, the connection of an external gate voltage to the QD energy level, effectively tunes the barrier potential created across the QD junction [47–49], which manifests a control over the nonreciprocity of JC [51–53]. Gupta *et al.* [51] have studied such effects in a three-terminal Josephson device using an external electrostatic gating. Moreover, in an InAs nanosheet-based JJ, suppression of the gate voltage dominates the current nonreciprocity [52, 53]. Along the same lines, theoretical approaches also predict the control over the unidirectional JC upon tuning the QD energy across a JJ [17, 19, 31], making it a noteworthy switching device. The anatomy of these properties of the QD has built the QD-based JD as an efficient tool for studying the quantum devices starting from quantum spin-qubits [27, 39, 54–56], transmon circuit [57], quantum interferometers [24, 58] and many more.

Of late, studies have advocated JDE in a driven JJ [50, 59]. Tarberner *et al.* [50] have shown the appearance of an anomalous JC (AJC) in a driven double QD-JJ leading to the CPR: $I(\phi = 0) \neq 0$, which is also explained as a ϕ_0 -JJ [26, 53, 60–62] in the literature. The appearance of this finite JC in the absence of any external SC phase bias causes an extra phase shift in the Josephson CPR as $I(\phi_0) = 0$ (i.e., the JC will become zero at $\phi = \phi_0 \neq 0$) which has been a consequence of the spin-orbit coupling and a magnetic field in a JJ [60, 61, 63–65]. The findings of AJC have set a new horizon to facilitate nonreciprocity in the context of Floquet-driven systems [50, 59]. However, in one of these studies [50], the Floquet drive is well-studied for the driven double QD JJ, albeit the exploration of the Majorana quasiparticles. Whereas, the other study [59] only shows the effect of two driven KCs coupled with each other without any intermediate weak link, leaving large possibilities to explore in detail.

Majorana physics [66–68] being the quintessential aspect of the topological JJ [32, 36, 46, 50, 69–78], the Floquet features have been exploited widely in Majorana-coupled JJ [50, 69, 74–77]. Furthermore, the appearance of the Majorana end modes, namely the Majorana 0-modes (MZMs) and the (Floquet) Majorana π -modes (MPMs) [69, 74–77] has validated the possibility of distinct topological quantum phases with different types of Majoranas. Influenced by Kitaev’s seminal work on one-dimensional (1D) model of a spinless p -wave superconductor [79] describing two spatially separated Majorana modes, the driven KC [59, 77, 80–86] has unfolded significant attributes of a driven JJ for exploring these Majoranas. Despite the exotic nature of p -wave superconductors, observable signatures, such as zero-bias conductance peaks [87–92] leads to unique nontrivial transport phenomena unattainable in junctions composed of conventional SC leads. Recently, within a similar genre, Kumari *et al.* [77] have examined the behaviour of the JC due to the unpaired Floquet-Majorana bound states in a JJ using the Floquet-Keldysh sum rule for the driven

superconductors and concluded with the robust predictions for a driven topological system. All these studies on Majorana JJ substantially enable the detection and control of the Majorana-bound states with great precision maintaining robustness against decoherence [93, 94]. Although Majorana-based JDE [32, 36, 46, 73] have been reported earlier, the diode signatures in those are induced by a Magnetic field and spin-orbit coupling. Thus, the evidence of an external field-free Majorana-JDE simply with a Floquet drive is scarce, which particularly motivates our present study.

The rationale behind conceiving the present investigation is multifold. Firstly, the role of the Floquet drive has not been established fully as an alternate tool to stimulate JDE, except for a few proposals [50, 59]. Secondly, though QD-based weak links between multiple KCs have been investigated in topological transport [50, 72, 95, 96], achieving the JDE has primarily focused on driving the QDs [50], instead of driving the KCs by operating them out of equilibrium, which could unveil novel phases (that are unattainable in static configurations). Furthermore, such an approach considering a driven QD lacks a clear physical realization of Majoranas, as the driving term effectively plays the role of a spin-orbit coupling in the QD rather than introducing new topological features. Thus, a driven QD does not alter the fundamental topological characteristics of the KC, thereby failing to generate the MPMs, which are essential signatures of Floquet-induced topology [97–100]. To the best of our knowledge, the hitherto proposals of the JDE (both Majorana and QD based) are achieved either in the presence of both an external magnetic field and Rashba spin-orbit interaction (for breaking the \mathcal{TRS} and \mathcal{IS} simultaneously), or with driven QDs. However, the search for a field-free Majorana-based JD still continues. In contrast, driven KCs demonstrate not only the enhancement of their inherent topological properties but also could introduce *artificial* spin-orbit coupling and Zeeman terms (playing the role of the external agents), which could result in richer nontrivial transport phenomena. Therefore, applying a Floquet drive to the KCs (keeping the QD as an undriven weak link) may be the simplest approach to achieve a JDE that should serve as a more physically meaningful and topologically enriched alternative to conventionally driven QD or external magnetic and spin-orbit field-based JD setups, which is our central aim.

The scarcity of such a QD-based JD with driven KCs intrigues the following questions:

- (i) Can a QD placed in between two driven KCs serve the same effect as that of an external field-free QD-based JD?
- (ii) Does the application of a Floquet drive to the SC lead of two p -wave KCs sufficient enough to break \mathcal{TRS} and \mathcal{IS} for achieving a finite rectification of the JD?
- (iii) How indispensable is the tuning of the RF upon varying the Floquet drive parameters and energy

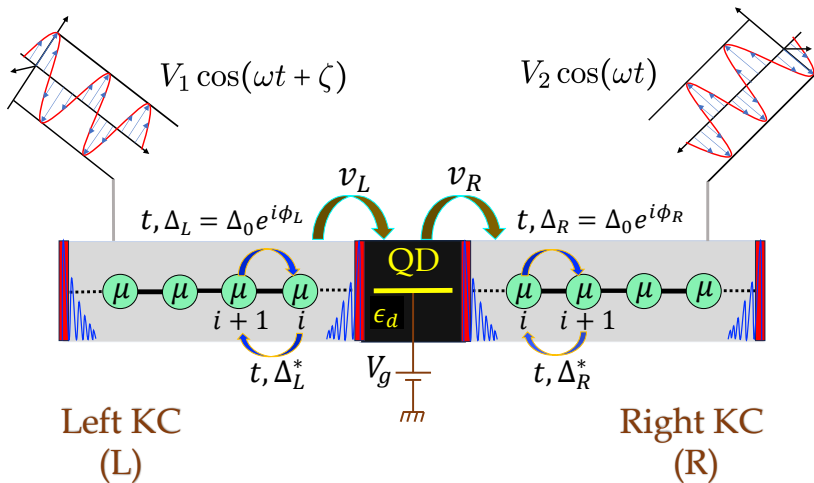


FIG. 1. A schematic illustration of a JJ composed of two p -wave spinless KCs with the chemical potential, μ , nearest-neighbour hopping strength, t , and the SC pairing potentials, Δ_L and Δ_R respectively for the left (L) and right (R) KCs connected via a QD-based weak link (highlighted in black) is presented. The SC phase difference, $\phi_L - \phi_R = \phi$, is maintained across the junction. The tunnelling amplitudes are denoted as v_L and v_R , corresponding to the L-QD and QD-R segments, respectively. The energy level of the QD, ϵ_d is tuned via an external gate voltage V_g . The Floquet version of this model is realized under the application of two periodic drives applied to the L and R KCs with a Floquet frequency, ω , accompanied by a finite phase difference, ζ . The Majorana modes are localized at the left and right edges of the KCs and also at the interfaces of the QD, which are denoted as red bars with their confined probability densities marked in blue lines.

level of the QD?

Therefore, it will be interesting to address some of these questions in the context of a KC-QD-KC type JJ and raise a proposition for a field-free QD-based Majorana JD.

With this motivation, we consider two periodically driven KCs coupled with an intermediate weak link of a QD that can capture this underlying physics of the JJ (schematically represented in Fig. 1) with the prospects of exploring the discipline of Majorana quasiparticles. Furthermore, inducing an asymmetric phase factor between the two Floquet drives associated with the two KCs may break \mathcal{TRS} and \mathcal{IS} , which in turn results in a finite nonreciprocity and rectification fulfilling the appropriate requirement of the diode effect. We also wish to investigate the impact of different system parameters, such as the chemical potential of the KCs, Floquet driving frequency, and the QD energy (tunable through a gate voltage), etc., on the diode's efficiency, which strongly influence the tunability of the diode effect. As the appearance of the Majorana end modes in the driven KC acts as a prototypical 1D spinless p -wave superconductor [79, 85, 88, 101–103], studying a JDE in such a KC-QD-KC based JJ may provide an understanding of quantum computations and spintronics applications [104].

A generic model of our diode setup is represented schematically in Fig. 1, where the description of the model is discussed in the figure caption. We organize the remainder of the paper as follows. In Sec. II, we present the static version of our model in which we introduce the static Hamiltonian in Sec. II A and briefly discuss

the essential physics of the MZMs and subsequently define the static JC in Sec. II B. Sec. III is devoted to the Floquet scenario hosting MPMs, which establishes the requirement of an asymmetric drive in breaking \mathcal{TRS} and \mathcal{IS} and generating a nonreciprocal current. Hence, we elaborately discuss the numerical results for the driven case, which includes the behaviour of the driven JC, its CPR characteristics, and the effects of the drive parameters on controlling the nonreciprocity of the driven JC in Sec. IV A, and examine the diode's efficiency in terms of the rectification factor in Sec. IV B both quantitatively and qualitatively. Sec. IV C explains the gate tunability of the diode effect. Finally, we summarize and conclude our findings in Sec. V.

II. STATIC KC-QD-KC JJ HOSTING MZMS

As mentioned, JJ requires a tunnel barrier that acts as a weak link between the two SC leads to conduct the flow of resistance-free supercurrent mediated via the Cooper pairs or other entities, such as Majoranas, as is the case here. In our model, we consider a semiconductor QD as the barrier (weak link), which is sandwiched between two finite spinless 1D p -wave KCs (acting as the SC leads), labeled as L(R) for the left(right) lead, forming a prototype for the JJ (as shown in Fig. 1). The static version of our model should be visualized without the drives that are depicted via the cosine modulations in Fig. 1. Experimental fabrication of the QD can be achieved by considering a single atom or single molecular structure [105] or

by stacking different semiconducting materials of uneven thicknesses between a source and a drain, producing a large potential barrier in a quantum well-like heterostructure [51]. In general, a QD can possess multiple quantized levels in which a given number of electrons can be accommodated because of this strong quantum confinement effect. However, in our study, we assume that the confinement effect is strong enough to cause sufficiently large level spacing. Hence, the QD can be viewed as a single spinful orbital, which is sufficiently relevant for the current to flow across the JJ. Furthermore, as said earlier, one may note that the discrete energy level of the QD is tunable by an external gate voltage V_g that may influence the transport through the QD. Therefore, the effect of V_g should be considered when deciphering the role of the QD in such a JJ setup.

A. Static Hamiltonian

Before delving into the scenario of a periodically driven JJ, we introduce the static (non-driven) Hamiltonian for our system that mimics a normal JJ and can be formulated as

$$\mathcal{H}_{\text{stat}} = \mathcal{H}_L + \mathcal{H}_R + \mathcal{H}_{\text{QD}} + \mathcal{H}_T, \quad (2)$$

where the components of $\mathcal{H}_{\text{stat}}$ are expressed as

$$\begin{aligned} \mathcal{H}_{L(R)} = & -\mu \sum_{j=1}^{N_s} c_{L(R),j}^\dagger c_{L(R),j} \\ & -t \sum_{j=1}^{N_s-1} \left[c_{L(R),j}^\dagger c_{L(R),j+1} + h.c. \right] \\ & + \sum_{j=1}^{N_s-1} \left[\Delta_{L(R)} c_{L(R),j+1}^\dagger c_{L(R),j} + h.c. \right], \quad (3) \end{aligned}$$

$$\mathcal{H}_{\text{QD}} = \sum_{\sigma} (\epsilon_d - eV_g) d_{\sigma}^{\dagger} d_{\sigma}, \quad (4)$$

$$\mathcal{H}_T = v_L c_{L,1}^{\dagger} d_{\sigma} + v_R c_{R,1}^{\dagger} d_{\sigma} + h.c., \quad (5)$$

which respectively represent the Hamiltonian for the left (right) KC (Eq. (3)), the central QD (Eq. (4)), and the tunnelling between KCs and the QD (Eq. (5)). In Eq. (3), the first term of $\mathcal{H}_{L(R)}$ denotes the onsite energy for the left (right) KC with μ being the chemical potential, and $c_{L(R),j}^{\dagger} (c_{L(R),j})$ being the creation (annihilation) operator of a spinless electron for the j -th site of each p -wave KC, while the second term signifies the nearest-neighbour (NN) hopping between two adjacent sites of the KC with

a coupling strength t . N_s represents the total number of sites for each KC. The SC pairing potential $\Delta_{L(R)}$ of the left (right) KC is designated by the third term of Eq. (3) which reads as $\Delta_{L(R)} = \Delta_0 e^{i\phi_{L(R)}}$, where Δ_0 and $\phi_{L(R)}$ denote the SC order parameter and the corresponding phase pertaining to the left (right) KCs, respectively. In Eq. (4), ϵ_d stands for a single quantized energy level of the QD, which can be tuned externally by a gate voltage V_g [53, 106]. $d_{\sigma}^{\dagger} (d_{\sigma})$ represents the creation (annihilation) operator for an electron present in the QD corresponding to the spin state, σ (\uparrow or \downarrow). It can be seen from Fig. 1 that the QD is coupled to the first ($j = 1$) site of each KC on either side, and hence the tunneling amplitudes of the left KC-to-QD and QD-to-right KC channels are designated by v_L and v_R , respectively in Eq. (5). To briefly encapsulate the conventional findings of a static QD-based JJ hosting MZMs and establish the requirement of a Floquet drive to achieve a nonreciprocal JC, we proceed as follows.

B. MZMs and static JC

At this point, it is crucial to understand the requisites of the p -wave KC and inspect the fate of the MZMs in such a QD-based heterojunction. To avoid the flow of discussions, we present the numerical variations and requisites of our static JJ model in Appendix A and B. In both the \mathcal{TRS} and particle-hole preserved classes, for a finite Δ_0 , the Majorana operators $(c_{L(R),j}^{\dagger} + c_{L(R),j})$ and $i(c_{L(R),j}^{\dagger} - c_{L(R),j})$ synthesize robust MZMs at the edges under an open boundary condition (OBC) provided the chemical potential (μ) of the KC satisfies $-2t < \mu < 2t$. In our study, the MZMs should appear across the junctions of the QD which can be analyzed by studying the behaviour of the energy spectrum and the static JC flowing through such a KC-QD-KC type JJ.

In order to establish this claim, we at first employ a canonical transformation, $e^{\mathcal{S}}$ with a unitary operator U to $\mathcal{H}_{\text{stat}}$, aiming to decouple the SC gap Δ_0 from the SC phase $\phi_{L(R)}$. Such a recipe simplifies the Hamiltonian and makes it more tractable to diagnose the system's behaviour in the presence of the SC phase. The generator \mathcal{S} that facilitates this transformation is given by [107]

$$\mathcal{S} = \sum_{j=1}^{N_s} \left[\frac{i\phi_L}{2} c_{L,j}^{\dagger} c_{L,j} + \frac{i\phi_R}{2} c_{R,j}^{\dagger} c_{R,j} \right]. \quad (6)$$

The transformed Hamiltonian, namely $\tilde{\mathcal{H}}_{\text{stat}} = e^{\mathcal{S}} \mathcal{H}_{\text{stat}} e^{-\mathcal{S}}$ reads as follows:

$$\tilde{\mathcal{H}}_{\text{stat}} = -\mu \sum_{\substack{\alpha \in L,R \\ j=1}}^{N_s} c_{\alpha,j}^{\dagger} c_{\alpha,j} + \sum_{\substack{\alpha \in L,R \\ j=1}}^{N_s-1} \left[-t c_{\alpha,j}^{\dagger} c_{\alpha,j+1} + \Delta_0 c_{\alpha,j+1}^{\dagger} c_{\alpha,j} + H.c. \right] + \mathcal{H}_{\text{QD}} + \sum_{\alpha \in L,R} \left[v_{\alpha} e^{i\frac{\phi_{\alpha}}{2}} c_{\alpha,1}^{\dagger} d_{\sigma} + H.c. \right]. \quad (7)$$

Under the above unitary transformation, the Hamiltonian of the central QD, \mathcal{H}_{QD} remains unaltered, while the SC phase $\phi_{L(R)}$ decouples entirely from the amplitude Δ_0 and appear only as a prefactor, $e^{i\frac{\phi_L}{2}} (e^{i\frac{\phi_R}{2}})$ in the tunnelling matrix elements. Thus, the decoupling scheme not only simplifies the model, but also captures the essential SC features of the leads in the tunnelling part itself, which helps to compute the SC phase difference induced JC for our system.

For convenience, we define the SC phase difference (ϕ) between the two KCs as $\phi = \phi_L - \phi_R$, referring to it as the ‘SC phase difference’ throughout. Referring to the variations of static energy spectra presented in Appendix A, it is confirmed that the localized MZMs at $E = 0$ are indeed present in our static model which ascertains that the inherent topology of the KC is still intact despite the presence of a QD. This serves as a benchmark for comparison and allows us to contrast our findings with the results reported previously [50, 72, 96].

With the topological characteristics being sorted out, we now define the static current for our model. To compute the static JC ($I(\phi)$) as a function of SC phase difference, ϕ , we use the eigenstates ($E_\gamma(\phi)$) of $\tilde{\mathcal{H}}_{\text{stat}}$ that satisfy $\tilde{\mathcal{H}}_{\text{stat}}(\phi)\psi_\gamma = E_\gamma(\phi)\psi_\gamma$ for the γ^{th} state. Then, the JC can be generically defined in terms of the Free-energy $F(\phi)$ and the Fermi distribution function, $f_\gamma = 1/2[1 - \tanh(E_\gamma/2k_B T)]$ as [23, 26, 32, 35, 36, 108]

$$I(\phi) = \frac{2e}{\hbar} \partial_\phi F(\phi), \quad F(\phi) = \sum_\gamma E_\gamma(\phi) f_\gamma. \quad (8)$$

For our system, summing over all the filled states below $E = 0$ (called as the ground state energy), the above ‘sum rule’ definition of current (8) at $T = 0$ simplifies to

$$I(\phi) = \frac{2e}{\hbar} \frac{\partial}{\partial \phi} E(\phi) = \frac{2e}{\hbar} \frac{\partial}{\partial \phi} \sum_{E_\gamma < 0} E_\gamma(\phi). \quad (9)$$

It is important to mention that $E(\phi)$ satisfies the symmetry relation $E(\phi) = E(-\phi)$, which stems from the transformation $\mathcal{U}\tilde{\mathcal{H}}_{\text{stat}}(\phi)\mathcal{U}^\dagger = \tilde{\mathcal{H}}_{\text{stat}}(-\phi)$. This implies that both $\tilde{\mathcal{H}}_{\text{stat}}(\phi)$ and $\tilde{\mathcal{H}}_{\text{stat}}(-\phi)$ share the same eigenvalues, ensuring that $E(\phi)$ remains an even function of ϕ (also shown in Fig. 14 in Appendix B). Consequently, the JC, $I(\phi)$, must be an odd function, which satisfies

$$I(\phi) = -I(-\phi), \quad (10)$$

which is evidently shown in the CPR of the static JC (Fig. 15 in Appendix B).

Thus, the equality of the JC identity in the static CPR reveals that the current is perfectly reciprocal, meaning that a finite diode effect cannot be realized in the static case unless the system is influenced with \mathcal{TRS} and \mathcal{IS} violations. For our purposes, as mentioned in Sec. I, rather than incorporating these additional ingredients, such as an external magnetic field or spin-orbit coupling, we aim to achieve an identical effect by driving the system out of

equilibrium. The impact of periodic driving and its role in modifying the transport properties will be explored in detail in the following sections.

III. DRIVEN SCENARIO

The junction, as described, does not inherently exhibit any non-reciprocal JC in the static KC-QD-KC heterojunction as the static Hamiltonian lacks explicit violation of \mathcal{TRS} or \mathcal{IS} . Typically, realizing a JDE necessitates one or more of the following: an external magnetic field [3, 4] or an intrinsic magnetic moment [17], magnetochiral anisotropy [15, 16] or a magnetic impurity [18, 41] to be present in the system to achieve a broken \mathcal{TRS} . In conjunction to obtain the broken \mathcal{IS} , typically the Rashba spin-orbit interaction [12, 13, 16, 19], a band asymmetry [45, 109] or a chiral property of the channel [9, 38, 42] has to be employed. However, here we prescribe a much simpler approach where the combined effects of a magnetic field and the spin-orbit interactions can effectively be replicated via driving the system into out-of-equilibrium scenarios, where a carefully chosen periodic modulation can effectively induce a finite nonreciprocity in the JC. In order to systematically capture these effects and make subsequent progress, we employ the Floquet formalism, which provides a powerful framework for analyzing any periodically driven system.

A. The Floquet formalism

We begin by introducing two harmonic drives of the same frequency (however maintaining a finite phase difference) applied to the onsite potentials of the two KCs (as presented in Fig. 1), which can be expressed as

$$\mathcal{H}_F(t) = \sum_{j=1}^{N_s} [V_1 \cos(\omega t + \zeta) c_{L,j}^\dagger c_{L,j} + V_2 \cos(\omega t) c_{R,j}^\dagger c_{R,j}]. \quad (11)$$

This term, together with Eq. (7), results in a total Hamiltonian for the KC-QD-KC model as

$$\mathcal{H}(t) = \tilde{\mathcal{H}}_{\text{stat}} + \mathcal{H}_F(t). \quad (12)$$

In Eq. (11), V_1 and V_2 represent the driving strengths, which we initially assume to have equal amplitudes, while ω denotes the driving frequency and ζ captures the phase difference between the two drives. Crucially, the asymmetry introduced by a nonzero ζ can break certain symmetries, thereby enabling the emergence of a diode effect in the system, a mechanism that we will explore in detail shortly. Before delving into that, we first provide a pedagogical overview of the Floquet formalism, which will allow us to derive a time-independent effective Hamiltonian for our analysis.

Floquet theory provides a systematic approach to solve the time-dependent Schrödinger equation by employing the Floquet ansatz, $|\psi(t)\rangle = e^{-iEt} |u(t)\rangle$, where

$|u(t + \mathcal{T})\rangle = |u(t)\rangle$ denotes the time-periodic Floquet states, and E represents the Floquet quasienergies. Analogous to quasi-momentum in crystalline solids, these quasienergies are periodic and confined within the Floquet Brillouin Zone, defined as, $E \in [-\pi/\mathcal{T} : \pi/\mathcal{T}]$ ($\mathcal{T} = 2\pi/\omega$, period of the drive). On the other hand, the Floquet modes can also be interpreted as the eigenstates of the Floquet stroboscopic time evolution operator ($\hat{U}(\mathcal{T})$) via

$$\begin{aligned} \hat{U}(\mathcal{T})|\psi(0)\rangle &= |\psi(\mathcal{T})\rangle, \\ \hat{U}(\mathcal{T})|u(0)\rangle &= e^{-iE\mathcal{T}}|u(\mathcal{T})\rangle = e^{-iE\mathcal{T}}|u(0)\rangle, \end{aligned} \quad (13)$$

with $\hat{U}(\mathcal{T})$ denoted by,

$$\hat{U}(\mathcal{T}) = \mathbb{T}\exp[-i \int_0^{\mathcal{T}} \mathcal{H}dt] = e^{-i\mathcal{H}_{\text{eff}}\mathcal{T}}. \quad (14)$$

Hence, \mathbb{T} denotes the time ordering product and \mathcal{H}_{eff} is the effective time-independent Hamiltonian. Eq. (11) fundamentally hosts an eigenvalue equation for the Floquet effective Hamiltonian, \mathcal{H}_{eff} , allowing the quasienergies to be obtained through exact diagonalization of the stroboscopic evolution operator in Eq. (14). This numerically requires a time-ordered decomposition of the evolution operator, which serves as a crucial step in extracting the Floquet effective Hamiltonian, given as,

$$\mathcal{H}_{\text{eff}} = \frac{i}{\mathcal{T}} \log[U(\mathcal{T}, 0)]. \quad (15)$$

This formulation provides a computationally efficient means to obtain a time-independent Floquet Hamiltonian while ensuring controlled approximation errors. Furthermore, in the context of a periodic drive, the time-averaged JC for a QD-based SC junction such as ours, can be evaluated with the help of the Floquet-eigenvalues ($E_{\mathcal{P}}$) of \mathcal{H}_{eff} as [77] (see Appendix. D)

$$I = \frac{1}{\mathcal{T}} \int_0^{\mathcal{T}} I(t')dt' = \frac{2e}{\hbar} \sum_{E_{\mathcal{P}} < 0} \partial_{\phi} E_{\mathcal{P}}. \quad (16)$$

B. Asymmetric Floquet drive: Breaking of \mathcal{TRS} and \mathcal{IS}

Before exploring the characteristics of the JC in the driven system and its role in inducing the nonreciprocal JC, it is essential to understand how periodic driving disrupts key symmetries by introducing longer-range interactions. In Fig. 2, we numerically compare the matrix configurations of the Hamiltonian for both the static and driven versions of the model, with a minimal setup comprising of only two lattice sites. The various elements of the matrix such as $\mu, t, \Delta_0, v_L, v_R$, etc. are color-coded according to their amplitudes, highlighting the structural modifications introduced by the drive. A key region of interest is the central block (confined within basis $d_{\uparrow}, d_{\downarrow}$), which corresponds to the QD. In the static

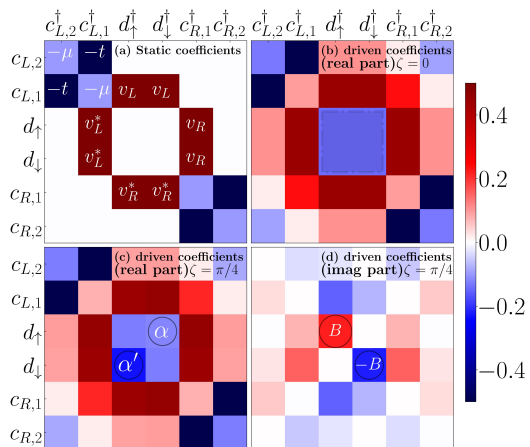


FIG. 2. The schematic representation of \mathcal{IS} and \mathcal{TRS} breaking using Floquet matrix. The figure illustrates matrix coefficients corresponding to static (panel a) and driven (panel b-c) version of the model in the coordinate basis ($c_{L,i}^{\dagger}, d_{\sigma}^{\dagger}, c_{R,i}^{\dagger}, \dots, c_{L,i}, d_{\sigma}, c_{R,i}$). In the driven case, as long as $\zeta \neq 0, \pi$, the system induces an artificial Zeeman $B(-B)$ and a spin-orbit-like terms $\alpha(\alpha')$, which emerge in the central block. This signifies the breakdown of \mathcal{IS} and \mathcal{TRS} at the central QD. The choice of parameters is indicated by the color bar, with the driving parameters set as $V_1 = V_2 = 1.5$, $\omega = 3$, and $\zeta = \pi/4$. We fix $\epsilon_d = V_g = 0$.

case (Fig. 2(a)), this block remains empty since the QD energy is set to zero. However, under periodic driving, additional longer-range interaction terms emerge, effectively filling up the central block, as depicted in Fig. 2(b). Notably, the effective Hamiltonian can host both real and imaginary components, each playing a distinct role in symmetry breaking. Focusing first on the real part, we observe that when the asymmetric phase ζ is varied from 0 to $\pi/4$, the two off-diagonal elements acquire different magnitudes (α and α'), resembling a spin-orbit-like interaction term that breaks \mathcal{IS} (Fig. 2(c)). Similarly, an inspection of the imaginary components reveals elements that are *not* completely zero, as they should have been in the static scenario, thus signalling a breakdown of \mathcal{TRS} . This is further confirmed by the presence of opposite signs for the diagonal elements in the central block, which can be interpreted as an artificial Zeeman field, B (Fig. 2(d)). Therefore, by tuning only one parameter, that is, ζ , one can selectively introduce terms in the Hamiltonian that can break both the \mathcal{IS} and \mathcal{TRS} , thereby enabling the emergence of diode-like characteristics in the driven system.

In the following section, we shall present the numerical results for the JC and examine how asymmetrically driven KCs induce a finite rectification, leading to the JDE. This naturally raises the question of whether a QD-based JJ, constructed from a pair of driven KCs, can also host distinct Floquet-Majorana modes. If such modes emerge, understanding their implications for transport properties becomes crucial. The answers to all of these

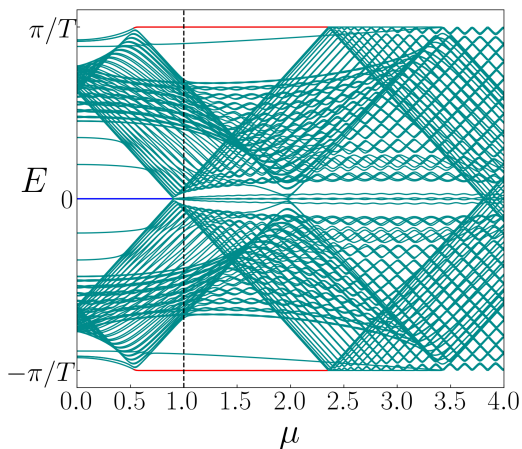


FIG. 3. Variations of the driven quasienergy spectrum, E (in units of t) as a function of the chemical potential of the KC, μ are shown for the drive amplitudes $V_1 = V_2 = 1.5$, the Floquet frequency, $\omega = 3$, and asymmetric phase factor, $\zeta = 0$. Other system parameters are set as $N_s = 20$, $\Delta_0 = 0.5$, $v_L = v_R = 0.5$, and $\epsilon_d = V_g = 0$. The quasienergies corresponding to the MZM and the two MPMs are marked in blue and red, respectively.

questions will become clear as we delve into the next section.

IV. NUMERICAL ANALYSIS OF PERIODICALLY DRIVEN JC AND DIODE CHARACTERISTICS

In this section, we present a comprehensive numerical analysis to explore the key characteristics of the JC, including its CPR, and the emergence of current non-reciprocity leading to a JDE under a driven scenario. For such an analysis, the system parameters are set as $N_s = 20$, $\Delta_0 = 0.5t$, $v_L = v_R = 0.5t$, and the driving amplitudes are chosen as $V_1 = V_2 = 1.5$. The JC is computed in units of $2e/\hbar$. These values have been kept constant throughout the paper. Further, all the energy parameters have been measured in units of the hopping strength (t), with t being set to unity. In addition, for simplicity, the QD energy (ϵ_d) is kept zero throughout and also the gate voltage is turned off until its effects are studied in Sec. IV C.

To begin with, since a well-defined topological phase is essential for our JJ model to obtain a finite JC, we highlight the inevitable role of periodic driving in enhancing the topological characteristics of the system in a driven scenario. Fig. 3 represents the quasienergy spectrum as a function of μ , with the Floquet frequency (ω) set as $\omega = 3$. The figure clearly describes the emergence of both the MZMs (which persist up to $\mu = 0.9$, marked by the blue line) and the MPMs (existing in the range $0.6 < \mu < 2.3$, marked by red lines). The presence of such localized edge states can be further validated by examining the probability distribution profile of the Majorana

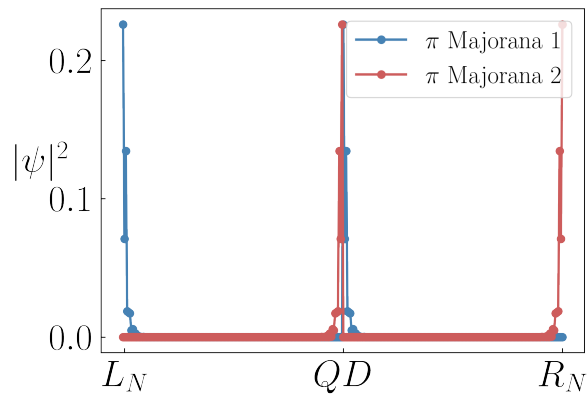


FIG. 4. The figure presents the probability distribution profile of MPMs that emerge at $\mu = 1$, as shown in Fig. 3, spanning a system of size $L = 4N_s + 4$. Regardless of the value of ϕ , four Majorana modes are always present, while two of them are localized at the edges of the entire system and the other two are confined at the interfaces of the QD, signifying the topological robustness. The remaining parameters are the same as in Fig. 3.

ana modes across the entire system, which we consider to be of length $L = 4N_s + 4$. Fig. 4 explicitly depicts the probability distribution of the π -modes at $\mu = 1$, revealing the existence of four MPMs. Among them, two resemble conventional MPMs, localized at the two ends of the chain, while the remaining two are confined at the interfaces of the QD. A similar localization pattern can also be observed for the MZMs as well (however not shown here). Interestingly, unlike hitherto reported findings [70, 110, 111] where the Majorana modes localized across the weak link could hybridize at specific values of ϕ , our model exhibits no such hybridization, ascertaining the unambiguous existence of the MPMs. This supports the robustness of these MPMs, ensuring that the persistence of a finite JC is entirely dictated by their survival.

A. Driven CPR, nonreciprocity and drive tunability

In accordance with Fig. 3, we begin by referring Fig. 5 which shows the CPR of the periodically driven JC (I) for three different values of μ at a particular drive frequency, namely $\omega = 3$. The rationale behind using such ω value is understood shortly afterwards. Here, for this plot, we have kept the asymmetric drive phase factor as $\zeta = 0$ because this analysis only allows us to delineate an optimal range of μ within which the system remains in the topological regime, facilitating further exploration of its transport characteristics. Like the static case, the time-averaged JC, I exhibits a 2π -periodicity with respect to the SC phase difference, ϕ . At this moment, it is worth mentioning the role of Majoranas on producing such a finite JC in the topological regime. From a technical standpoint, the system retains its topological nature

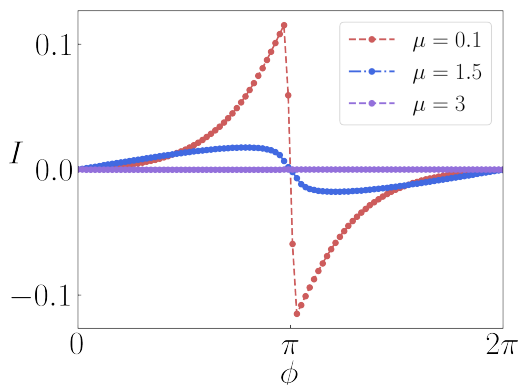


FIG. 5. The driven CPR in terms of the time-averaged JC, I (in units of $2e/h$) vs. the SC phase difference ϕ is plotted at a particular Floquet frequency, $\omega = 3$ for different values of the chemical potential, μ of the KC. Other system parameters are the same as those in Fig. 3. Further, we set $\zeta = 0$. This figure demonstrates that I remains nonzero till the distinct Majorana modes survive for specific ranges of μ . For $\mu = 0.1$, I exhibits a finite discontinuity at $\phi = \pi$ hosting MZMs (similar to the static case), while MPMs influence I for $\mu = 1.5$, and finally I becomes zero in the trivial regime ($\mu > 2.3$) for $\mu = 3$.

up to $\mu = 2.3$ (as described in Fig. 3), meaning that any chemical potential within this range guarantees a finite JC, which can also be confirmed from Fig. 5. Specifically, as suggested from Fig. 3, for $\mu = 0.1$, where only the MZMs exist, a finite JC is carried by the corresponding Majorana modes, accompanied by a finite ‘jump’ at $\phi = \pi$. The appearance of this ‘jump’ is similar to the static case caused due to the cumulative effects of higher harmonics and linear E - ϕ variation around $\phi = \pi$, as discussed in Appendix A. Similarly, at $\mu = 1.5$, despite the absence of MZMs, the presence of localized MPMs enables the transport of a finite JC, albeit with diminishing of the abrupt discontinuity and making it more like a sinusoidal variation. However, as for $\mu > 2.3$ the system enters into a trivial phase, the JC corresponding to $\mu = 3$ becomes zero, preventing any current flow in the KC-QD segment. Therefore, we infer that the driven JC remains nonzero as long as the MPMs survive in the driven scenario (in range $\mu \in [0.6 : 2.3]$ as shown in Fig. 3). Interestingly, referring to the explicit variation of the π -Majorana current (displayed in Fig. 17) corresponding to the MPM dispersion (Fig. 16(b)) presented in Appendix C, we conclude that the individual current contribution coming purely from a π -energy mode is negligibly small compared to the total bulk JC shown in Fig. 5. This comparative observation between the bulk and the Majorana JC fundamentally corroborates that the flow of the JC is conducted only through the Majorana end modes (albeit their own contribution to the JC is negligible), without which the JC ceases to exist in a KC-QD-KC type JJ, implying the topological robustness of the Majorana mediated transport.

To envisage the effects of the driving parameters, such

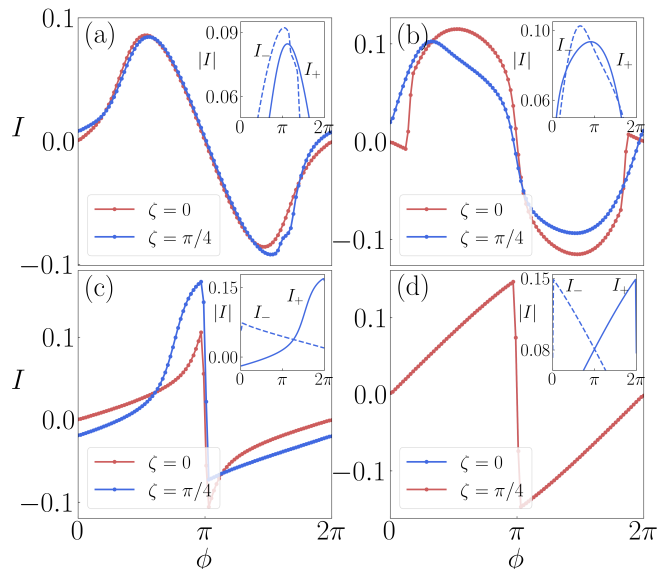


FIG. 6. Time-averaged JC, I (in units of $2e/h$) vs. SC phase difference ϕ at zero and finite asymmetric Floquet drive parameter (ζ) is plotted at $\zeta = 0$ and $\zeta = \pi/4$ labeled by red and blue lines, respectively for lower to higher Floquet frequencies ω as: (a) $\omega = 0.8$, (b) $\omega = 2$, (c) $\omega = 3$, and (d) $\omega \geq 5$. The insets (plotted for $|I|$ of the blue curves at $\zeta \neq 0$) represent the disparity between two differently directed currents, namely I^+ and I^- designated by solid and dotted blue lines, respectively. Insets of Figs.(a)-(c) signify prominent disparity between I^+ and I^- in the lower to intermediate range of ω , which ceases to exist in Fig.(d) at high ω reaching the static limit. Other system parameters are fixed as $N_s = 20$, $V_1 = V_2 = 1.5$, $\Delta_0 = 0.5$, $v_L = v_R = 0.5$, $\epsilon_d = V_g = 0$, and $\mu = 0.5$.

as the Floquet drive frequency (ω) and asymmetric drive factor (ζ) on the CPR of the driven current (I), we plot Fig. 6. It illustrates the 2π -periodic CPR of the time-averaged JC, I for different regimes of driving frequencies, both for zero and nonzero ζ , labeled by red and blue lines, respectively. We first examine the case where $\zeta = 0$. It is expected that in the high-frequency regime, the system behaves similarly to its static counterpart (Appendix A), resulting in a CPR characterized by a linear E - ϕ relation, which in turn leads to an abrupt ‘jump’ at $\phi = \pi$ (Fig. 6(d)). A similar behaviour is observed at certain intermediate frequencies, such as $\omega = 3$ (see Fig. 6(c)). In contrast, for lower frequencies, such as $\omega = 0.8$ (Fig. 6(a)) and $\omega = 2$ (Fig. 6(b)), the JC deviates significantly from the static case, and instead exhibits a nearly sinusoidal profile. This deviation stems from the hybridization of the Floquet sidebands, which eliminates the crossing of MZMs energy, thereby smearing out the abrupt jumps in the current at $\phi = \pi$ and consequently, the JC follows a nearly sinusoidal pattern in the lower regimes of ω . Nonetheless, time-averaging over a sufficiently long period ultimately restores the regular sinusoidal pattern of the JC [112].

A more fundamental and prime aspect of our investigation is to achieve the nonreciprocity of JC, which leads

to a finite diode rectification for which the breaking of both \mathcal{TRS} and \mathcal{IS} are mandatory. It is discussed elaborately in Sec. III B that introducing an additional phase difference between the two drives, namely, ζ can effectively generate an artificial magnetic field and a spin-orbit-like terms in the Hamiltonian (which is evident in Fig. 2) which leads to the breaking of these symmetries. Hence, we study the effect of ζ , specifically for $\zeta = \pi/4$ (the choice for such ζ -value will be clear as we proceed) on CPR of the driven JC. Together, the artificial Zeeman and spin-orbit terms cause an imbalance in the dynamics of Majorana quasiparticles moving in opposite directions, that is forward moving pair can experience a different effective velocity with respect to the oppositely moving pairs. This directional dependency of current leads to an inequality in the critical currents [26, 108], expressed as $I_c^+ \neq I_c^-$, where $I_c^+ = \max(I(\phi))$ and $I_c^- = \min(I(\phi))$, with + and - signs denoting the direction of the current. Consequently, the CPR becomes asymmetric satisfying

$$I(\phi) \neq -I(-\phi), \quad (17)$$

which can be vividly seen in Fig. 6, denoted by the red line plots. A closer examination of Fig. 6 (insets of Fig. 6(a)-(c)) further highlights the relative difference between I_c^+ and I_c^- , which plays a crucial role in quantifying the nonreciprocity in terms of the diode RF (defined in Eq. (1)). This is the central result of our study. However, before concluding the findings of Fig. 6 and analyzing the diode characteristics explicitly by estimating the RF, we comment on a few more crucial attributes of the driven CPR for completeness.

Although the driven JC deviates from a purely sinusoidal form in both low and intermediate frequency regimes (Fig. 6(a)-(c)), yet it gives rise to an anomalous ϕ_0 -JC [26, 50, 53, 59–62], that is $I(\phi)$ attains a nonzero value at $\phi = 0, \pi$ whenever the asymmetric phase factor is nonzero. As it is known that ϕ_0 -JJ is likely to be realized in presence of the Zeeman and spin-orbit coupling terms [26, 53, 60–62], the plausible occurrence of ϕ_0 -JJ (especially for $\omega < 5$) characteristics in our study is therefore mediated through a nonzero ζ . This is also a direct consequence of the broken \mathcal{TRS} and \mathcal{IS} phenomenon caused by ζ presented in Fig. 2. Hence, we can refer a JC for a nonzero ζ (excluding $n\pi$ where $n = \pm 1, \pm 2, \dots$) and a given frequency range (preferably ω lying in low to intermediate regimes) to as the anomalous ϕ_0 -JC satisfying a finite JC in the absence of the SC phase difference.

Since, our primary interest lies in exploring the behavior of the JC at frequencies where it deviates from the static case, revealing unique transport phenomena that are otherwise inaccessible, we focus on $\omega = 3$ for the following discussion. Fig. 7 displays how the driven JC varies with the different values of the asymmetric phase factor ζ . Notably, the current satisfies $I_c^+ = I_c^-$ only when ζ takes integer multiples of π ($n\pi$, where n is an integer) including zero, corroborating the vanishing of the nonreciprocity. Furthermore, the current profiles for $\zeta = 0$ and

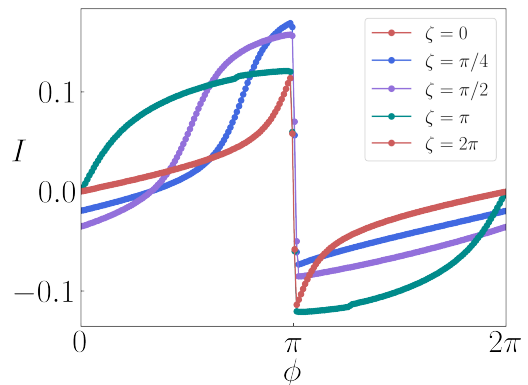


FIG. 7. The driven CPR in terms of the time-averaged JC, I (in units of $2e/h$) vs. the SC phase difference ϕ is plotted at a particular Floquet frequency, $\omega = 3$ for different values of the asymmetric Floquet drive parameter, ζ . Other system parameters are fixed as those in Fig. 6. The current does not render any nonreciprocity when $\zeta = n\pi$ ($n = 0, \pm 1, \pm 2, \dots$). However, for intermediate values of ζ , such as $\zeta = \pi/4$, it shows a finite nonreciprocity.

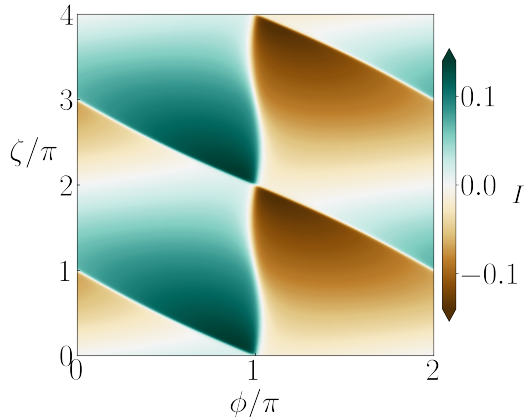


FIG. 8. A contour plot of the time-averaged JC, I (in units of $2e/h$) is shown in the $\zeta - \phi$ plane (scaled by π) for a particular Floquet frequency, $\omega = 3$. Other system parameters are fixed as those in Fig. 6. The current is 2π periodic with respect to both ϕ and ζ . For specific values of ζ , I remains purely non-sinusoidal, supporting the nonreciprocity. Hence, the tunability of the nonreciprocity is controlled by the drive parameters.

$\zeta = 2\pi$ perfectly overlap with each other, indicating that the JC exhibits a 2π -periodicity not only in ϕ but also in ζ . In contrast, for intermediate values such as $\zeta = \pi/4$ and $\pi/2$, the current largely deviates from the sinusoidal behavior (maintaining the discontinuity as it shown in Fig. 6 for an intermediate regime of ω) and more importantly there exists a significant distinction between I_c^+ and I_c^- , which ensures the existence of nonreciprocity in the driven picture for these values of ζ . Because of this reason, we (mostly) fix ζ at $\zeta = \pi/4$ whenever needed for our numerical analysis. Further, to gain a more comprehensive understanding, we plot the phase diagram of the

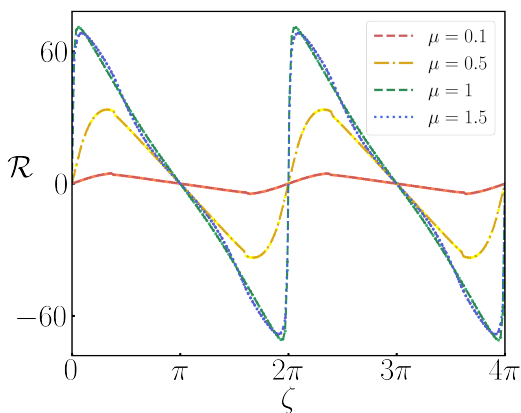


FIG. 9. Variations of the diode RF (\mathcal{R}) as a function of the asymmetric Floquet drive parameter, ζ are displayed for different values of the chemical potential (μ) of the KCs at a chosen Floquet frequency, $\omega = 3$. Other system parameters are fixed as those in Fig. 6. It is shown that \mathcal{R} exhibits a sawtooth variation, and it is 2π -periodic with respect to ζ . Furthermore, \mathcal{R} undergoes a sign reversal at every π interval of ζ , which can also be understood from Fig. 8. The maximum \mathcal{R} achieved for this range of μ is around 70% at specific values of ζ .

JC in the ζ - ϕ plane in Fig. 8. The results confirm that for specific values of ζ , which are relevant for the nonreciprocity, the JC remains purely non-sinusoidal, yet periodic with respect to both ϕ and ζ . Moreover, extending the analysis to negative values of ζ reveals an important symmetry relation of the time-averaged current I with respect to ϕ and ζ as

$$I(\phi, \zeta) = -I(-\phi, -\zeta), \quad \forall \zeta \neq 0. \quad (18)$$

These findings in this section conclude that we can significantly tune the nonreciprocity according to the choice of driving parameters, ω and ζ .

B. Diode efficiency: Rectification factor

By this time, we have established the notion of a finite nonreciprocity of JC (solely induced by the asymmetric phase factor, ζ of the Floquet drive) in our system which is further responsible for the JDE. Now, in this section, we explicitly estimate how *efficient* such a KC-QD-KC type JD can be owing to this nonreciprocity. Recalling the fact that for any value of ζ (excluding $\zeta = \pm n\pi$), there exists a notable disparity between I_c^+ and I_c^- , which fundamentally ascertains the emergence of the JDE. This observation naturally motivates to scrutinize the diode RF, $\mathcal{R} = (I_c^+ - |I_c^-|) / (I_c^+ + |I_c^-|)$, following Eq. 1.

As ζ is the main driving agent for generating a finite RF, we present Fig. 9 to investigate how \mathcal{R} varies as a function of ζ for different values of the chemical potential μ at a fixed Floquet frequency, ω . However, we keep the QD parameters fixed as $\epsilon_d = V_g = 0$. The dependence of

\mathcal{R} on μ points to a sawtooth-like variation as a function of ζ regardless of the choice of μ . However, the magnitude of \mathcal{R} increases with increasing μ , yet its oscillatory behavior with respect to ζ remains consistent and reaches a maximum of \mathcal{R} . Hence, our inspection reveals that the maximum \mathcal{R} , namely \mathcal{R}_{\max} can be achieved around $\mathcal{R}_{\max} \sim 70\%$ for our KC-QD-KC JJ at $\zeta = (2n\pi \pm \pi/8)$ provided μ and the driving parameters (ζ and ω) are preferably chosen. However, it is important to note that the presence of a finite V_g can significantly vary \mathcal{R} (both qualitatively and quantitatively) for these values of μ .

Another key feature is that the 2π -periodic \mathcal{R} (with respect to ζ) changes its sign at every π interval of ζ . This sign reversal of \mathcal{R} can be further verified through the contour plot of I in the ϕ - ζ plane (Fig. 8), which clearly shows that at each π -interval of ζ , the JC acquires an additional π phase. This leads to a crucial relation in the RF satisfying

$$\mathcal{R}(\zeta) = -\mathcal{R}(\zeta + \pi). \quad (19)$$

Thus, we conclude that ζ not only plays a key role in producing a finite JDE, but also acts as a tuning parameter (responsible for the sign reversal of \mathcal{R}) for setting the biasing condition, offering an effective means of controlling the JDE.

To gain deeper insight into how the diode effect operates across different frequency regimes, it is essential to analyze the RF as a function of Floquet frequency, ω . Fig. 10 presents the variation of \mathcal{R} with ω for four distinct values of μ . As said earlier, the asymmetric drive parameter, ζ is fixed at $\pi/4$ for our analysis. A noteworthy observation from this figure is that regardless of the choice of μ , \mathcal{R} exhibits irregular fluctuations in the low-frequency regime. In contrast, as ω increases \mathcal{R} reaches a peak for each of these values of μ (exhibiting a maximum of \mathcal{R} around 70% for $\mu = 1.5$) at a certain ω (ω_p), before undergoing a linear decline in the intermediate-frequency regime (the frequency range where μ is comparable to ω). This linear dependence indicates that within this regime of ω , the JC should exhibit a smooth and periodic variation. Consequently, RF gradually decreases and eventually vanishes in the high-frequency regime, which is expected in the static limit. Hence, this notable feature implies that the transition from a finite to a zero value of \mathcal{R} occurs at a critical, ω (say ω_s) which shifts to a greater value for larger values of μ . Moreover, as μ increases, the rate of decline in rectification in the intermediate-frequency regime gets slower, exhibiting a larger difference between ω_p and ω_s . Therefore, for larger values of μ , ω_s is required to be larger for the RF to vanish. This analysis demonstrates a high-precision smooth operating region for the JD by controlling the frequency ω and the asymmetric drive strength ζ .

In summary, by appropriately tuning both ζ and ω , one can effectively control and optimize the RF based on the specific requirements. Moreover, the ability to modulate rectification through external driving parameters could be instrumental in designing high-efficiency SC circuits,

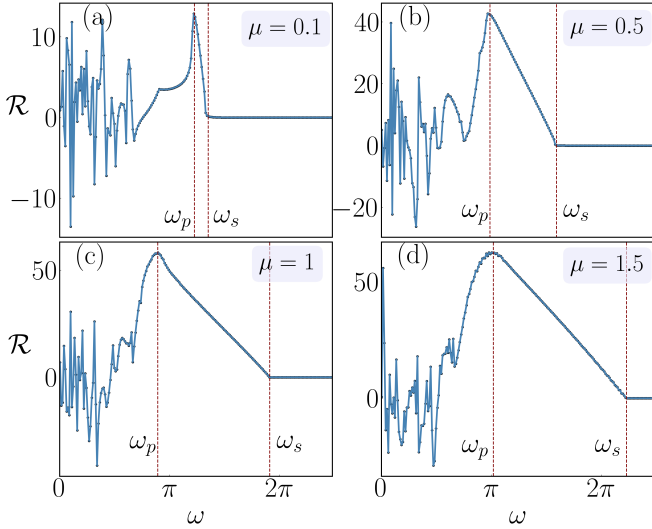


FIG. 10. Dependence of the RF (\mathcal{R}) on the Floquet frequency, ω is displayed for different values of the chemical potential (μ) as (a) $\mu = 0.1$, (b) $\mu = 0.5$, (c) $\mu = 1$, (d) $\mu = 1.5$. Here, ζ is fixed at $\pi/4$. Other system parameters are fixed as those in Fig. 6. These variations reveal that for each case of μ , \mathcal{R} exhibits a peak at a certain $\omega = \omega_p$ accompanied by oscillations in the lower ω range, and then declines linearly in the intermediate ω range and finally becomes zero at $\omega = \omega_s$ where it reaches the static limit. The rate of decline is different for different values of μ .

non-reciprocal quantum devices, and next-generation SC electronics.

C. Gate tunability of the diode effect

So far, we have discussed the effects of an asymmetric drive in elucidating the occurrence of a finite rectification for such a Majorana coupled JD. It is also crucial to understand the importance of a QD playing the role of a weak link in the context of a JD. As pointed out earlier, the discrete energy level of the QD (ϵ_d) can be adjusted through electrostatic gating [47–49] which offers a precise control on JC [12, 19, 31, 41, 50–52], enabling a fine-tuning of the critical current and the phase dynamics. Therefore, it is essential to examine how the QD energy level, (tuned by a gate voltage V_g) can impact both the JC and the RF. The application of the gate electrode effectively modifies ϵ_d to $\epsilon'_d = \epsilon_d - eV_g$, which further suggests that eV_g can act as a rescaled QD energy. That is true even if $\epsilon_d = 0$ as kept throughout this study. Another important aspect of utilizing the QD as the weak link is its ability to act as a discrete resonant level and to cause successive on and off resonances with respect to the Fermi-energy (chemical potential, μ) of the KCs (SC leads) [113, 114]. This significantly influences the periodic modulation of the JC and hence the RF. Thus, this control of level-matching feature through tuning V_g is the key to manifest transport aided by the Majoranas

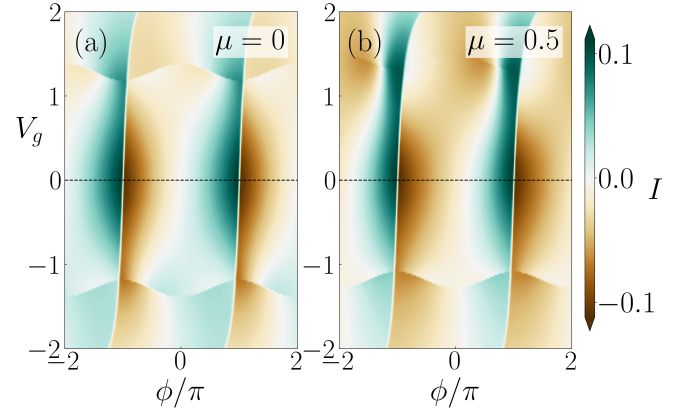


FIG. 11. The combined effects of an external gate voltage (V_g) and the chemical potential (μ) on the time-averaged JC, I is displayed in a contour plot, where I (in units of $2e/\hbar$) is plotted in the $V_g - \phi$ plane for a particular Floquet frequency, $\omega = 3$, and asymmetry phase factor $\zeta = \pi/4$. Panel (a) shows the scenario for $\mu = 0$, while panel (b) shows that for $\mu = 0.5$. Other system parameters are set as those in Fig. 6. This plot reveals a symmetry relation of I given as $I(\phi, V_g) = -I(-\phi, -V_g)$ which holds only when $\mu = 0$ (Fig.(a)). However, for $\mu \neq 0$, a clear disparity in the current profile between the upper and lower halves of $V_g = 0$ line is noticed (Fig.(b)), implying this identity to be invalid.

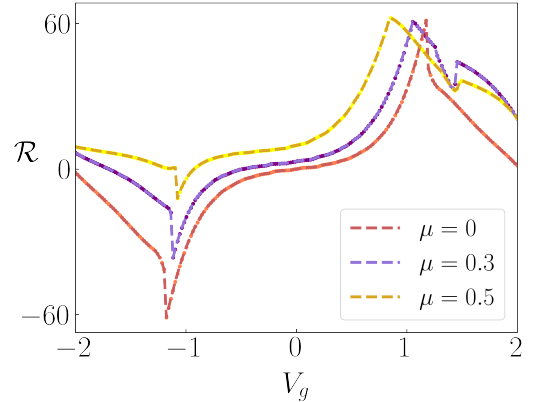


FIG. 12. The figure illustrates the variation of \mathcal{R} as a function of an external gate voltage, V_g , for different values of the chemical potential, μ at a particular Floquet frequency, $\omega = 3$, and asymmetry phase factor $\zeta = \pi/4$. The rest of the system parameters are chosen similarly to as mentioned in Fig. 6. Clearly, \mathcal{R} has a symmetric pattern with respect to $V_g = 0$ only when $\mu = 0$. Moreover, \mathcal{R} increases with increasing V_g . The fine adjustment of μ and V_g determines the tunability of the JD and hence the optimization of \mathcal{R} .

across such QD based JJ. Therefore, tuning V_g becomes necessary to exploit the role of the QD on the JC and hence the diode's RF.

To begin with, we explore the CPR as a function of V_g . For the analyses presented in Fig. 11, the parameters are chosen exactly the same as those kept in Sec. IV A. At this stage, it is essential for us to recall that to sustain a

finite JC, eV_g must lie within the SC gap, $2\Delta_0$ [113, 114], i.e., $V_g \in [-1, 1]$ corresponding to the SC gap chosen as $\Delta_0 = 0.5$. However, this condition does not appear to be entirely true in the driven scenario since in a Floquet system, the SC gap is no longer fixed at $\Delta_0 = 0.5$, instead evolves to an effective gap, namely Δ_0^{eff} , whose magnitude depends on both the strength and frequency of the drive. Therefore, for a given choice of $\Delta_0 = 0.5$, we fix the range of V_g as $-2 \leq V_g \leq 2$ accordingly for generating the contour plot for I in the V_g - ϕ plane in Fig. 11 and also for the variations of \mathcal{R} for different values of μ . A careful examination of Fig. 11(a) reveals a key identity persistent in the time-averaged current, given by

$$I(\phi, V_g) = -I(-\phi, -V_g) \quad \text{iff} \quad \mu = 0. \quad (20)$$

As Eq. (20) suggests, this symmetry with respect to $V_g = 0$ (as shown in Fig. 11(a)) holds only when the chemical potential (μ) is identically equal to zero. Any deviation from $\mu = 0$ causes a disparity in the current profile (higher contribution along positive V_g axis for $\mu > 0$) around $V_g = 0$, thereby rendering Eq. (20) as invalid at those values of μ which can be understood from Fig. 11(b).

Further, by taking this into account, we analyze the variation of \mathcal{R} as a function of V_g for different values of μ at $\zeta = \pi/4$ which is illustrated in Fig. 12. As anticipated, much like the JC, \mathcal{R} retains its symmetry around $V_g = 0$ for $\mu = 0$ and adheres to the relation: $\mathcal{R}(V_g) = -\mathcal{R}(-V_g)$. Interestingly, akin to the behaviour of I , the symmetry of \mathcal{R} around $V_g = 0$ also gets disrupted (accompanied by an upward shift in \mathcal{R}) accordingly when μ deviates from zero (shown in violet and yellow dotted lines). Our findings indicate that a finite rectification effect persists within an extended window of $V_g \in [-2 : 2]$ in the driven case. Furthermore, within this range μ , the maximum rectification $\mathcal{R}_{\text{max}} \approx 70\%$, can also be achieved, albeit at a finite V_g . However, \mathcal{R}_{max} can be enhanced further by increasing μ or by choosing a different set of parameters (not shown here). The enhancement of the RF with $|V_g|$ for $\mu \neq 0$ indicates a better degree of resonance between the Fermi energy of the KC leads (μ) and the QD energy ($\sim -eV_g$). However, beyond a certain $|V_g|$, the barrier potential across the QD caused by this level mismatch dominates over the flow of JC, rendering a decrease in I and hence in the RF. Thus, the interplay between μ and V_g strongly influences the current dynamics and the diode efficiency. In summary, both the JC and \mathcal{R} exhibit a periodic dependence on V_g (provided $\mu = 0$), and we have successfully identified an optimal range of V_g where a substantial and hence technologically significant (tunable) diode effect can be realized.

V. SUMMARY AND CONCLUSION

To summarize, we investigate the JDE under the application of an asymmetric Floquet drive to the two 1D p -wave KCs (acting as two SC leads) and a QD (playing the role of a weak link) sandwiched between them,

mimicking a prototype for a KC-QD-KC type JJ. We began by introducing the static version of our model and briefly discussed the essential topological physics of localized MZMs in the static spectrum. Defining the static JC by summing over all the negative energy states of the static Hamiltonian, we show that the static JJ lacks nonreciprocity and the CPR satisfies $I(\phi) = -I(-\phi)$. This is expected as neither a \mathcal{TRS} breaking external agents nor an \mathcal{IS} breaking spin-orbit coupling effect is included, which could induce a finite nonreciprocity for our JJ setup. It turns out that an asymmetric Floquet drive serves the purpose of symmetry breaking, meaning if we apply a periodic drive to the KCs (SC-leads) with different phases (referred to as asymmetric phase factor ζ), \mathcal{TRS} and \mathcal{IS} are broken simultaneously. Thereafter, incorporating such asymmetric drive into our static model, we compute the time-averaged JC using the Floquet formalism and explicitly establish the emergence of \mathcal{TRS} and \mathcal{IS} breaking phenomenon (explained through the spectral representation of the Floquet matrix components in Fig. 2). Following the definition of the driven current, we then numerically calculate the behaviour of the time-averaged JC (I) and elaborately investigate its key CPR characteristics in different regimes of chemical potential (μ) of the KC, the Floquet frequency (ω) and the asymmetric phase factor (ζ). At first, we decipher a preferred range of μ to access the essential topological effects of the MPMs in asserting a nonzero JC and hence study the explicit dependence of CPR of the driven JC on ζ in different ω regimes. The numerical analyses reveal that our system can host MPMs in the range $0.6 < \mu < 2.3$ (established through the driven quasienergy spectra and probability density) to validate the topological aspects of Majorana modes in mediating a finite JC. As expected, the driven JC exhibits 2π -periodic CPR, similar to that for the static JC. The central outcome of our study is realized as soon as we turn on the asymmetric phase factor, ζ which notably distinguishes the disparity between the forward (I^+) and the reverse (I^-) JC (satisfying $I^+ \neq I^-$) owing to the simultaneous breaking of \mathcal{TRS} and \mathcal{IS} , which leads to a finite nonreciprocity and rectification. Additionally, the application of ζ brings in other important attribute of the JJ phenomena, such as a ‘‘anomalous JJ CPR’’ or ϕ_0 -JC satisfying $I(\phi = 0, \pi) \neq 0$ and a non-sinusoidal pattern of JC, relevant for attaining a finite nonreciprocity for our diode setup.

Next, we quantify the efficiency of our KC-QD-KC type diode for various system parameters. The explicit variation of \mathcal{R} as a function of ζ reveals its 2π -periodic sawtooth behaviour along with a sign change characteristic at every π -interval of the phase ζ satisfying $\mathcal{R}(\zeta) = -\mathcal{R}(\zeta + \pi)$. Our results conclude that the chemical potential of the KCs and the driving parameters play a crucial role in determining the largest possible RF for the Floquet-driven JD. Gate tunability of the QD energy level additionally modulates the diode RF. By judiciously choosing the system parameters, the maximum RF can be achieved around $\mathcal{R} \sim 70\%$ for our diode setup.

Thus, our study suggests that all these system parameters strongly influence the tuning and optimizing of the diode efficiency.

From the experimental realization, the QD can be fabricated using semiconductors [47–49], such as GaAs, InSb, etc., or a single ‘adatom’ (metallic or non-metallic nature) acting as a JJ weak link. By controlling the radius of the QD (under strong confinement effects), the single energy level can be attained which is further tunable by electrostatic gating [47–49, 113, 114]. Following the experimental observation of Majorana in the past [115, 116] recent works on the realization of minimal KC using an array of QDs [117, 118] have been put forward to validate the existence of the topological Majorana modes. The appearance of these end modes through an InSb nanowire [92] strongly coupled to QDs includes proximity-induced superconductivity, which can be studied by elastic co-tunnelling (ECT) and crossed Andreev reflection (CAR) [117]. Hence, the experimental setup for our model can be designed using a Nb sheet [92] or ceramics, such as $\text{YBa}_2\text{Cu}_3\text{O}_7$ (YBCO) as the bulk and by using STM-probe [119] magnetic atoms or QDs with magnetic impurities could be deposited on the bulk superconductor like an array of adatoms that induces Majorana modes at the ends of the KC [120, 121]. Furthermore, a nonmagnetic adatom/QD can be placed in between two KCs to construct the JJ setup. Applying two different ac voltage drives [122] to the KC or using a photonic simulator [123], one can generate an asymmetric Floquet drive, by which the modulation of the KCs’ chemical potential can be achieved. Finally, connecting a dc source to the intermediate QD will help tune the gate voltage. Consideration of different materials according to the experimental requirement is viable.

To conclude, though attempts have been made to establish a diode effect either induced by different magnetic and spin-orbit coupling effects or by a Floquet drive (to the intermediate weak link, i.e., to the QD), our Floquet-driven KC-based JJ not only assists in engineering a non-reciprocal supercurrent associated with topological Majorana modes, but also rules out the need for any externally applied magnetic or spin-orbit coupling components. Therefore, our study underscores an alternative proposition of a QD-based JD, replacing the conventional usage of such external factors via driven KCs, which will aid in realizing Majorana-mediated quantum transport in SC devices and quantum computation.

ACKNOWLEDGMENTS

We sincerely thank Prof. Diptiman Sen for his valuable comments and suggestions. D.D. acknowledges the Department of Space (DoS), Government of India for all the support at the Physical Research Laboratory and the Department of Physics, IIT Guwahati for the local hospitality during her visit to pursue this work. D.D. also thank P. Dutta for her encouragement and support. K.B. ac-

knowledges the Science and Engineering Research Board (SERB), Govt. of India, for providing financial support through the National Post Doctoral Fellowship (NPDF) (File No. PDF/2023/000161).

Appendix A: Static energy spectrum vs. μ

The MZMs, being one of the fundamental characteristics of a KC can be visualized in the energy spectrum of the entire system under OBC which is obtained by diagonalizing the transformed Hamiltonian (7).

For $\phi_{L(R)} = 0$ and π , $\mathcal{H}_{L(R)}$ preserves both the \mathcal{TRS} : $\mathcal{T}\mathcal{H}_{L(R)}\mathcal{T}^\dagger = \mathcal{H}_{L(R)}$ and the particle-hole symmetry (PHS): $\mathcal{C}\mathcal{H}_{L(R)}\mathcal{C}^\dagger = -\mathcal{H}_{L(R)}$ (\mathcal{C} being an anti-unitary operator that typically acts as complex conjugation (\mathcal{K}) in the Majorana basis. These symmetries refer to the ‘‘BDI’’ topological class, while for $\phi_{L(R)} \neq 0, \pi$ it only obeys PHS which belongs to the topological ‘‘D’’ class [80, 124].

As at $\phi = \pi$, both \mathcal{TRS} and PHS are preserved, the variation of the total static energy (E) with respect to the chemical potential of the KC, μ (see Fig. 13) demonstrates that despite the presence of a weak link (such as a QD) in between two KCs, the MZMs are indeed present as localized modes at $E = 0$. The existence of localized MZM states across the junctions of the QD can also be verified by the probability distribution plotted at the sites of the system (however not shown here).

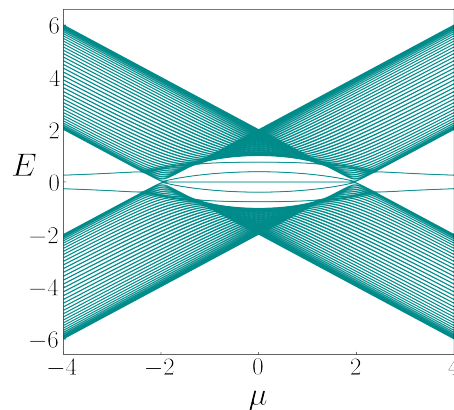


FIG. 13. Variations of the static energy spectrum, E (in units of t) with respect to the chemical potential of the KC, μ is shown for the system parameters being set as $N_s = 20$, $\Delta_0 = 0.5$, $\epsilon_d = V_g = 0$, and $v_L = v_R = 0.5$.

Appendix B: Static E - ϕ variation and CPR

Fig. 14 presents the E - ϕ dispersion exhibiting 2π -periodicity with respect to the SC phase difference ϕ for a chemical potential ($\mu = 0.5$) within the topological regime provided $\mu < |2t|$, as mentioned in Sec. II B. The E - ϕ variation presented here clearly illustrates the emergence of

localized MZMs at $E = 0$. These pieces of evidence collectively signify the robustness of the underlying topological traits of the KC in the presence of a QD for the static version of our model.

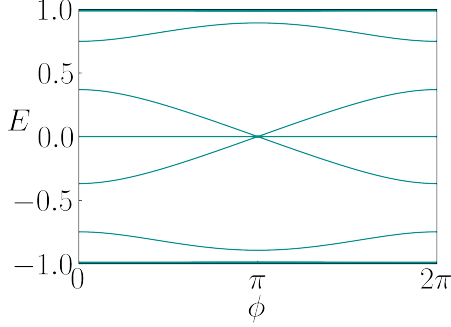


FIG. 14. Variation of the static energy spectrum, E as a function of the SC phase difference, ϕ has been shown for the system parameters chosen as similar to those in Fig. 13.

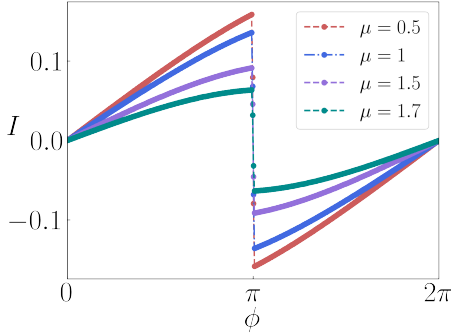


FIG. 15. The static JC, $I(\phi)$ (in units of $2e/\hbar$), is shown as a function of the SC phase difference ϕ , with parameter $N_s = 20$, $\Delta_0 = 0.5$, $v_L = 0.9$, $v_R = 0.5$, $\epsilon_d = V_g = 0$, for the chemical potentials $\mu = 0.5, 1.0, 1.5$, and 1.7 .

Following the definition in Eq. (9), we compute static $I(\phi)$ and explicitly plot its CPR for different values of μ in Fig. 15. As expected, $I(\phi)$ behaves as an odd function of ϕ satisfying Eq. 10. Additionally, the E - ϕ dispersion in the vicinity of $\phi = \pi$ exhibits a linear behavior caused by the crossing of the MZMs energy states around $\phi = \pi$, manifesting a zigzag pattern in the current profile [70, 71] accompanied by a finite discontinuity at $\phi = \pi$, rather than showing a purely sinusoidal form. Notably, this behavior remains consistent at all values of μ as long as the system remains in the topological regime. Another important observation is that the magnitude of the JC gradually decreases as μ increases.

Appendix C: Role of MPMs on driven CPR

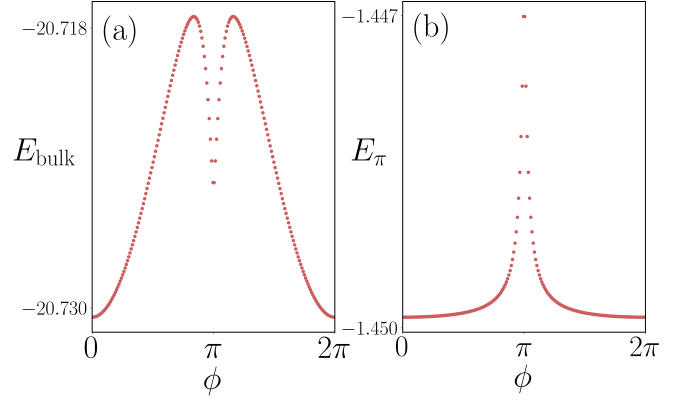


FIG. 16. The Bulk and the π -Majorana E - ϕ dispersion (in units of $2e/\hbar$) is plotted for Floquet frequency, $\omega = 3$ and for $\zeta = \pi/4$. Other system parameters are fixed as those in Fig. 6.

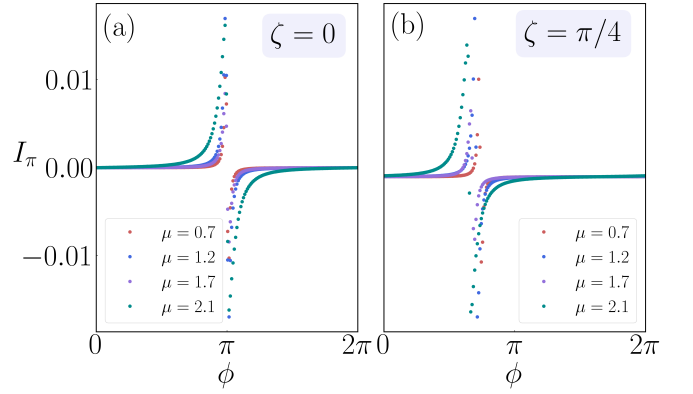


FIG. 17. The driven CPR for the MPMs in terms of the π -mode current, I_π (in units of $2e/\hbar$) vs. the SC phase difference ϕ is displayed at a particular Floquet frequency, $\omega = 3$ for (a) $\zeta = 0$ and (b) $\zeta = \pi/4$. Other system parameters are fixed as those in Fig. 6.

The signatures of MPMs being entrenched by the Floquet drive as displayed in Fig. 3, here we explicitly show the E - ϕ dispersion of the bulk and also that of a distinct MPM in Fig. 16 (a) and (b) labeled as E_{bulk} and E_π , respectively. Interestingly, while the E - ϕ dispersion remains linear in the static case (Fig. 14), resulting in a zigzag current profile (Fig. 15), the driven system exhibits significant deviations due to the hybridization of multiple Floquet sidebands occurring only at lower or intermediate frequencies such as $\omega = 3$, which in turn modifies the energy of the JJ.

To study the driven JC that arises purely from the localized MPMs, we plot Fig. 17 which presents the CPR for $\zeta = 0$ and $\zeta = \pi/4$, specifically focusing on the contribution from the π -energy modes of the driven spectrum

(the lowest energy state in Fig. 3). The π -Majorana current, denoted as I_π , is computed within a range of μ where these modes persist. Because of a gap closing in the driven quasienergy spectrum at $\phi = \pi$ there exists a sharp kink that gives rise to an infinite discontinuity in the corresponding current profile (see Fig. 17(a)). This discontinuity consistently appears at $\phi = \pi$, regardless of the choice of μ . However, upon introducing a finite ζ , the kink in the E - ϕ diagram, and consequently, the discontinuity in I_π shifts from $\phi = \pi$ to $\phi = \pi - \zeta$ as shown in Fig. 17(b). Importantly, this shift remains fixed at these values of ϕ and independent of μ as long as the system remains in the topological regime. Furthermore, due to this intrinsic discontinuity at $\phi = \pi$, I_π remains perfectly reciprocal, implying that the current associated with Majorana states does not contribute to the nonreciprocity. Additionally, the magnitude of I_π for MPMs is significantly smaller compared to the total JC shown in Figs. 5-7. This observation suggests that although the contribution in the JC profile coming from the Majorana modes is negligible, their presence is needed to maintain the topological robustness during the passage of current from the left KC to the right KC through the QD.

Appendix D: Operator form of driven JC

The current operator can be written in terms of the steady-state density matrix, $\rho(t)$ and the Floquet states

$u_{\mathcal{P}}(t)$ as,

$$\begin{aligned} \hat{I}(t) &= \text{Tr}(\rho(t)\partial_\phi\mathcal{H}(t)) = \sum_{\mathcal{P}} \langle u_{\mathcal{P}}(t)|\rho(t)\partial_\phi\mathcal{H}(t)|u_{\mathcal{P}}(t) \rangle \\ &= \sum_{\mathcal{P}\mathcal{Q}} \langle u_{\mathcal{P}}(t)|\rho(t)|u_{\mathcal{Q}}(t) \rangle \langle u_{\mathcal{Q}}(t)|\partial_\phi\mathcal{H}(t)|u_{\mathcal{P}}(t) \rangle. \end{aligned} \quad (\text{D1})$$

Using $\langle u_{\mathcal{P}}(t)|\rho(t)|u_{\mathcal{Q}}(t) \rangle \approx n_{\mathcal{P}}\delta_{\mathcal{P}\mathcal{Q}}$, where $n = \sum_m f(\epsilon_{\mathcal{P}} + m\omega)\langle u_{\mathcal{P}}^m|u_{\mathcal{P}}^m \rangle$ which is ultimately unity for our system (as $T = 0$), Eq. (D1) yields

$$\hat{I}(t) = \sum_{\mathcal{P}} \langle u_{\mathcal{P}}(t)|\partial_\phi\mathcal{H}(t)|u_{\mathcal{P}}(t) \rangle. \quad (\text{D2})$$

Now, time-averaging Eq. (D2), we obtain

$$\begin{aligned} I &= \frac{1}{T} \int_0^T \sum_{\mathcal{P}} [\langle u_{\mathcal{P}}(t)|\partial_\phi(\mathcal{H}(t))|u_{\mathcal{P}}(t) \rangle \\ &\quad - \langle u_{\mathcal{P}}(t)|\mathcal{H}(t)|\partial_\phi u_{\mathcal{P}}(t) \rangle] \\ &= \sum_{\mathcal{P}} \partial_\phi \epsilon_{\mathcal{P}}, \end{aligned} \quad (\text{D3})$$

which follows Eq. (16).

-
- [1] F. Braun, “Ueber die stromleitung durch schwefelmetalle,” *Annalen der Physik* **229**, 556–563 (1875).
 - [2] W. Shockley, *Electrons and Holes in Semiconductors: With Applications to Transistor Electronics*, Bell Telephone Laboratories series (Van Nostrand, 1950).
 - [3] F. Ando, Y. Miyasaka, T. Li, J. Ishizuka, T. Arakawa, Y. Shiota, T. Moriyama, Y. Yanase, and T. Ono, “Observation of superconducting diode effect,” *Nature* **584**, 373–376 (2020).
 - [4] E. Strambini, M. Spies, N. Ligato, S. Ilić, M. Rouco, C. González-Orellana, M. Ilyn, C. Rogero, F. Bergeret, J. Moodera, *et al.*, “Superconducting spintronic tunnel diode,” *Nature communications* **13**, 2431 (2022).
 - [5] H. Narita, J. Ishizuka, R. Kawarazaki, D. Kan, Y. Shiota, T. Moriyama, Y. Shimakawa, A. V. Ognev, A. S. Samardak, Y. Yanase, *et al.*, “Field-free superconducting diode effect in noncentrosymmetric superconductor/ferromagnet multilayers,” *Nature Nanotechnology* **17**, 823–828 (2022).
 - [6] A. Daido, Y. Ikeda, and Y. Yanase, “Intrinsic superconducting diode effect,” *Phys. Rev. Lett.* **128**, 037001 (2022).
 - [7] T. de Picoli, Z. Blood, Y. Lyanda-Geller, and J. I. Väyrynen, “Superconducting diode effect in quasi-one-dimensional systems,” *Phys. Rev. B* **107**, 224518 (2023).
 - [8] J.-X. Hu, Z.-T. Sun, Y.-M. Xie, and K. T. Law, “Josephson diode effect induced by valley polarization in twisted bilayer graphene,” *Phys. Rev. Lett.* **130**, 266003 (2023).
 - [9] B. Zinkl, K. Hamamoto, and M. Sigrist, “Symmetry conditions for the superconducting diode effect in chiral superconductors,” *Phys. Rev. Res.* **4**, 033167 (2022).
 - [10] S. Banerjee and M. S. Scheurer, “Enhanced superconducting diode effect due to coexisting phases,” *Phys. Rev. Lett.* **132**, 046003 (2024).
 - [11] Y. Yerin, S.-L. Drechsler, A. A. Varlamov, M. Cuoco, and F. Giazotto, “Supercurrent rectification with time-reversal symmetry broken multiband superconductors,” (2024), [arXiv:2404.12641](https://arxiv.org/abs/2404.12641) [cond-mat.supr-con].
 - [12] J. S. Meyer and M. Houzet, “Josephson diode effect in a ballistic single-channel nanowire,” (2024), [arXiv:2404.01429](https://arxiv.org/abs/2404.01429) [cond-mat.mes-hall].
 - [13] H. F. Legg, D. Loss, and J. Klinovaja, “Superconducting diode effect due to magnetochiral anisotropy in topological insulators and rashba nanowires,” *Phys. Rev. B* **106**, 104501 (2022).
 - [14] Y. Tokura and N. Nagaosa, “Nonreciprocal responses from non-centrosymmetric quantum materials,” *Nat. Commun.* **9**, 3740 (2018).
 - [15] C. Baumgartner, L. Fuchs, A. Costa, S. Reinhardt, S. Gronin, G. C. Gardner, T. Lindemann, M. J. Manfra, F. J. P. E., D. Kochan, J. Fabian, N. Paradiso, and C. Strunk, “Supercurrent rectification and magnetochiral effects in symmetric josephson junctions,” *Nature Nanotechnology* **17**, 39–44 (2022).

- [16] L. Bauriedl, C. Bäuml, L. Fuchs, C. Baumgartner, N. Paulik, J. M. Bauer, K.-Q. Lin, J. M. Lupton, T. Taniguchi, K. Watanabe, C. Strunk, and N. Paradiso, “Supercurrent diode effect and magnetochiral anisotropy in few-layer nbse₂,” *Nature Communications* **13**, 4266 (2022).
- [17] D. Debnath and P. Dutta, “Field-free josephson diode effect in interacting chiral quantum dot junctions,” (2024), [arXiv:2411.18325 \[cond-mat.supr-con\]](https://arxiv.org/abs/2411.18325).
- [18] Y.-F. Sun, Y. Mao, and Q.-F. Sun, “Design of josephson diode based on magnetic impurity,” *Phys. Rev. B* **108**, 214519 (2023).
- [19] D. Debnath and P. Dutta, “Gate-tunable josephson diode effect in rashba spin-orbit coupled quantum dot junctions,” *Phys. Rev. B* **109**, 174511 (2024).
- [20] A. Soori, “Josephson diode effect in one-dimensional quantum wires connected to superconductors with mixed singlet-triplet pairing,” *Journal of Physics: Condensed Matter* **37**, 10LT02 (2025).
- [21] B. Josephson, “Possible new effects in superconductive tunnelling,” *Physics Letters* **1**, 251–253 (1962).
- [22] K. Misaki and N. Nagaosa, “Theory of the nonreciprocal josephson effect,” *Phys. Rev. B* **103**, 245302 (2021).
- [23] Y. Zhang, Y. Gu, P. Li, J. Hu, and K. Jiang, “General theory of josephson diodes,” *Phys. Rev. X* **12**, 041013 (2022).
- [24] R. S. Souto, M. Leijnse, and C. Schrade, “Josephson diode effect in supercurrent interferometers,” *Phys. Rev. Lett.* **129**, 267702 (2022).
- [25] Y.-J. Wei, H.-L. Liu, J. Wang, and J.-F. Liu, “Supercurrent rectification effect in graphene-based josephson junctions,” *Phys. Rev. B* **106**, 165419 (2022).
- [26] M. Davydova, S. Prembabu, and L. Fu, “Universal josephson diode effect,” *Science Advances* **8**, eabo0309 (2022).
- [27] Y. V. Fominov and D. S. Mikhailov, “Asymmetric higher-harmonic squid as a josephson diode,” *Phys. Rev. B* **106**, 134514 (2022).
- [28] B. Lu, S. Ikegaya, P. Buset, Y. Tanaka, and N. Nagaosa, “Tunable josephson diode effect on the surface of topological insulators,” *Phys. Rev. Lett.* **131**, 096001 (2023).
- [29] H. Huang, T. de Picoli, and J. I. Väyrynen, “Superconducting diode effect in two-dimensional topological insulator edges and josephson junctions,” *Applied Physics Letters* **125**, 032602 (2024).
- [30] P. Chatterjee and P. Dutta, “Quasiparticles-mediated thermal diode effect in weyl josephson junctions,” *New Journal of Physics* **26**, 073035 (2024).
- [31] Q. Cheng and Q.-F. Sun, “Josephson diode based on conventional superconductors and a chiral quantum dot,” *Phys. Rev. B* **107**, 184511 (2023).
- [32] J. F. Steiner, L. Melischek, M. Trahms, K. J. Franke, and F. von Oppen, “Diode effects in current-biased josephson junctions,” *Phys. Rev. Lett.* **130**, 177002 (2023).
- [33] S. Fracassi, S. Traverso, N. Traverso Ziani, M. Carrega, S. Heun, and M. Sassetti, “Anomalous supercurrent and diode effect in locally perturbed topological josephson junctions,” *Applied Physics Letters* **124** (2024).
- [34] P. Zalom, M. Žonda, and T. Novotný, “Hidden symmetry in interacting-quantum-dot-based multiterminal josephson junctions,” *Phys. Rev. Lett.* **132**, 126505 (2024).
- [35] C.-X. Liu, A. M. Bozkurt, F. Zatelli, S. L. ten Haaf, T. Dvir, and M. Wimmer, “Enhancing the excitation gap of a quantum-dot-based kitaev chain,” *Communications Physics* **7**, 1–12 (2024).
- [36] J. Cayao, N. Nagaosa, and Y. Tanaka, “Enhancing the josephson diode effect with majorana bound states,” *Phys. Rev. B* **109**, L081405 (2024).
- [37] H. Wu, Y. Wang, Y. Xu, P. K. Sivakumar, C. Pasco, U. Filippozzi, S. S. P. Parkin, Y.-J. Zeng, T. McQueen, and M. N. Ali, “The field-free josephson diode in a van der waals heterostructure,” *Nature* **604**, 653–656 (2022).
- [38] K. Chen, B. Karki, and P. Hosur, “Intrinsic superconducting diode effects in tilted weyl and dirac semimetals,” [arXiv:2309.11501](https://arxiv.org/abs/2309.11501) (2023).
- [39] W. Yu, J. J. Cuzzo, K. Sapkota, E. Rossi, D. X. Rademacher, T. M. Nenoff, and W. Pan, “Time reversal symmetry breaking and zero magnetic field josephson diode effect in dirac semimetal Cd₃As₂ mediated asymmetric squids,” *Phys. Rev. B* **110**, 104510 (2024).
- [40] D. Chakraborty and A. M. Black-Schaffer, “Perfect superconducting diode effect in altermagnets,” (2024), [arXiv:2408.07747 \[cond-mat.supr-con\]](https://arxiv.org/abs/2408.07747).
- [41] M. Trahms, L. Melischek, J. F. Steiner, B. Mahendru, I. Tamir, N. Bogdanoff, O. Peters, G. Reecht, C. B. Winkelmann, F. von Oppen, and K. J. Franke, “Diode effect in josephson junctions with a single magnetic atom,” *Nature* **615**, 628–633 (2023).
- [42] J. J. He, Y. Tanaka, and N. Nagaosa, “The supercurrent diode effect and nonreciprocal paraconductivity due to the chiral structure of nanotubes,” *Nature Communications* **14**, 3330 (2023).
- [43] B. Turini, S. Salimian, M. Carrega, A. Iorio, E. Strambini, F. Giazotto, V. Zannier, L. Sorba, and S. Heun, “Josephson diode effect in high-mobility insb nanoflags,” *Nano Lett.* **22**, 8502–8508 (2022).
- [44] T. Liu, M. Smith, A. V. Andreev, and B. Z. Spivak, “Giant nonreciprocity of current-voltage characteristics of noncentrosymmetric superconductor–normal metal–superconductor junctions,” *Phys. Rev. B* **109**, L020501 (2024).
- [45] A. Soori, “Josephson diode effect in junctions of superconductors with band asymmetric metals,” (2023), [arXiv:2312.14084 \[cond-mat.supr-con\]](https://arxiv.org/abs/2312.14084).
- [46] Z. Liu, L. Huang, and J. Wang, “Josephson diode effect in topological superconductors,” *Phys. Rev. B* **110**, 014519 (2024).
- [47] A. P. Alivisatos, “Semiconductor clusters, nanocrystals, and quantum dots,” *Science* **271**, 933–937 (1996).
- [48] A. M. J. Zwerver, T. Krähenmann, T. F. Watson, L. Lampert, H. C. George, R. Pillarisetty, S. A. Bojarski, P. Amin, S. V. Amitonov, J. M. Boter, R. Caudillo, D. Correas-Serrano, J. P. Dehollain, G. Droulers, E. M. Henry, R. Kotlyar, M. Lodari, F. Lüthi, D. J. Michalak, B. K. Mueller, S. Neyens, J. Roberts, N. Samkharadze, G. Zheng, O. K. Zietz, G. Scappucci, M. Veldhorst, L. M. K. Vandersypen, and J. S. Clarke, “Qubits made by advanced semiconductor manufacturing,” *Nature Electronics* **5**, 184–190 (2022).
- [49] G. Burkard, T. D. Ladd, A. Pan, J. M. Nichol, and J. R. Petta, “Semiconductor spin qubits,” *Rev. Mod. Phys.* **95**, 025003 (2023).
- [50] C. Ortega-Taberner, A.-P. Jauho, and J. Paaske, “Anomalous josephson current through a driven double

- quantum dot,” *Phys. Rev. B* **107**, 115165 (2023).
- [51] M. Gupta, G. Graziano, M. Pendharkar, J. T. Dong, C. P. Dempsey, C. Palmström, and V. S. Pribiag, “Gate-tunable superconducting diode effect in a three-terminal josephson device,” *Nat. Commun.* **14** (2023).
- [52] S. Yan, Y. Luo, H. Su, H. Gao, X. Wu, D. Pan, J. Zhao, J.-Y. Wang, and H. Xu, “Gate tunable josephson diode effect in josephson junctions made from inas nanosheets,” (2025), arXiv:2501.15523 [cond-mat.mes-hall].
- [53] W. Mayer, M. C. Dartiaill, J. Yuan, K. S. Wickramasinghe, E. Rossi, and J. Shabani, “Gate controlled anomalous phase shift in al/inas josephson junctions,” *Nature communications* **11**, 212 (2020).
- [54] D. Loss and D. P. DiVincenzo, “Quantum computation with quantum dots,” *Phys. Rev. A* **57**, 120–126 (1998).
- [55] J. J. Cuzzo, W. Pan, J. Shabani, and E. Rossi, “Microwave-tunable diode effect in asymmetric squids with topological josephson junctions,” *Phys. Rev. Res.* **6**, 023011 (2024).
- [56] A. Greco, Q. Pichard, E. Strambini, and F. Giazotto, “Double loop dc-squid as a tunable josephson diode,” (2024), arXiv:2404.05521 [cond-mat.supr-con].
- [57] A. Bargerbos, M. Pita-Vidal, R. Žitko, J. Ávila, L. J. Splitthoff, L. Grünhaupt, J. J. Wesdorp, C. K. Andersen, Y. Liu, L. P. Kouwenhoven, R. Aguado, A. Kou, and B. van Heck, “Singlet-doublet transitions of a quantum dot josephson junction detected in a transmon circuit,” *PRX Quantum* **3**, 030311 (2022).
- [58] C. Ciaccia, R. Haller, A. C. C. Drachmann, T. Lindemann, M. J. Manfra, C. Schrade, and C. Schönberger, “Gate-tunable josephson diode in proximitized inas supercurrent interferometers,” *Phys. Rev. Res.* **5**, 033131 (2023).
- [59] A. Soori, “Anomalous josephson effect and rectification in junctions between floquet topological superconductors,” *Physica E: Low-dimensional Systems and Nanostructures* **146**, 115545 (2023).
- [60] A. Zazunov, R. Egger, T. Jonckheere, and T. Martin, “Anomalous josephson current through a spin-orbit coupled quantum dot,” *Phys. Rev. Lett.* **103**, 147004 (2009).
- [61] T. Yokoyama, M. Eto, and Y. V. Nazarov, “Anomalous josephson effect induced by spin-orbit interaction and zeeman effect in semiconductor nanowires,” *Phys. Rev. B* **89**, 195407 (2014).
- [62] A. Assouline, C. Feuillet-Palma, N. Bergeal, T. Zhang, A. Mottaghizadeh, A. Zimmers, E. Lhuillier, M. Edrrie, P. Atkinson, M. Aprili, *et al.*, “Spin-orbit induced phase-shift in bi2se3 josephson junctions,” *Nature communications* **10**, 126 (2019).
- [63] A. Buzdin, “Direct coupling between magnetism and superconducting current in the josephson φ_0 junction,” *Phys. Rev. Lett.* **101**, 107005 (2008).
- [64] I. V. Krive, A. M. Kadigrobov, R. I. Shekhter, and M. Jonson, “Influence of the rashba effect on the josephson current through a superconductor/luttinger liquid/superconductor tunnel junction,” *Phys. Rev. B* **71**, 214516 (2005).
- [65] A. A. Reynoso, G. Usaj, C. A. Balseiro, D. Feinberg, and M. Avignon, “Anomalous josephson current in junctions with spin polarizing quantum point contacts,” *Phys. Rev. Lett.* **101**, 107001 (2008).
- [66] J. Alicea, “New directions in the pursuit of majorana fermions in solid state systems,” *Reports on Progress in Physics* **75**, 076501 (2012).
- [67] C. Beenakker, “Search for majorana fermions in superconductors,” *Annual Review of Condensed Matter Physics* **4**, 113–136 (2013).
- [68] M. Leijnse and K. Flensberg, “Introduction to topological superconductivity and majorana fermions,” *Semiconductor Science and Technology* **27**, 124003 (2012).
- [69] A. Kundu and B. Seradjeh, “Transport signatures of floquet majorana fermions in driven topological superconductors,” *Phys. Rev. Lett.* **111**, 136402 (2013).
- [70] J. Cayao, P. San-Jose, A. M. Black-Schaffer, R. Aguado, and E. Prada, “Majorana splitting from critical currents in josephson junctions,” *Physical Review B* **96**, 205425 (2017).
- [71] L. Baldo, L. G. G. V. Dias Da Silva, A. M. Black-Schaffer, and J. Cayao, “Zero-frequency supercurrent susceptibility signatures of trivial and topological zero-energy states in nanowire junctions,” *Superconductor Science and Technology* **36**, 034003 (2023).
- [72] D. T. Liu, J. Shabani, and A. Mitra, “Long-range kitaev chains via planar josephson junctions,” *Phys. Rev. B* **97**, 235114 (2018).
- [73] Y.-M. Gao, H. Xiao, M.-H. Jiang, F. Chi, Z.-C. Yi, and L.-M. Liu, “Josephson diode effect in parallel-coupled double-quantum dots connected to unalike majorana nanowires,” *Nanomaterials* **14** (2024), 10.3390/nano14151251.
- [74] C. Peng, A. Haim, T. Karzig, Y. Peng, and G. Refael, “Floquet majorana bound states in voltage-biased planar josephson junctions,” *Phys. Rev. Res.* **3**, 023108 (2021).
- [75] D. T. Liu, J. Shabani, and A. Mitra, “Floquet majorana zero and π modes in planar josephson junctions,” *Phys. Rev. B* **99**, 094303 (2019).
- [76] D. Wang, Z. Ding, M. Li, Y. Tao, and H. Fu, “Explicit-time floquet topological superconductivity in a microwave/infrared frequency ac voltage-driven josephson junction,” *Phys. Rev. Res.* **6**, 023059 (2024).
- [77] R. Kumari, B. Seradjeh, and A. Kundu, “Josephson-current signatures of unpaired floquet majorana fermions,” *Phys. Rev. Lett.* **133**, 196601 (2024).
- [78] S. D. Escribano, A. E. Dahl, K. Flensberg, and Y. Oreg, “Phase-controlled minimal kitaev chain in multiterminal josephson junctions,” (2025), arXiv:2501.14597 [cond-mat.mes-hall].
- [79] A. Y. Kitaev, “Unpaired majorana fermions in quantum wires,” *Phys. Usp.* **44**, 131 (2001).
- [80] Q.-J. Tong, J.-H. An, J. Gong, H.-G. Luo, and C. H. Oh, “Generating many majorana modes via periodic driving: A superconductor model,” *Phys. Rev. B* **87**, 201109 (2013).
- [81] M. Thakurathi, K. Sengupta, and D. Sen, “Majorana edge modes in the kitaev model,” *Phys. Rev. B* **89**, 235434 (2014).
- [82] H.-Y. Wang, L. Zhuang, and W. M. Liu, “Majorana edge modes of kitaev chain with multiple time periodic driving,” (2019), arXiv:1910.10911 [cond-mat.mes-hall].
- [83] K. Roy, S. Roy, and S. Basu, “Quasiperiodic disorder induced critical phases in a periodically driven dimerized p-wave kitaev chain,” *Scientific Reports* **14** (2024), 10.1038/s41598-024-70995-2.

- [84] K. Roy and S. Basu, “Single and multifrequency driving protocols in a rashba nanowire proximitized to an s -wave superconductor,” *Physical Review B* (2024).
- [85] R. M. Lutchyn, J. D. Sau, and S. D. Sarma, “Majorana fermions and a topological phase transition in semiconductor-superconductor heterostructures,” *Phys. Rev. Lett.* **105**, 077001 – Published 13 August, 2010 **105**, 077001 (2010).
- [86] H. Wu, S. Wu, and L. Zhou, “Floquet topological superconductors with many majorana edge modes: topological invariants, entanglement spectrum and bulk-edge correspondence,” *New Journal of Physics* **25**, 083042 (2023).
- [87] K. T. Law, P. A. Lee, and T. K. Ng, “Majorana fermion induced resonant andreev reflection,” *Physical Review Letters* **103**, 237001 (2009).
- [88] A. Das, Y. Ronen, Y. Most, Y. Oreg, M. Heiblum, and H. Shtrikman, “Zero-bias peaks and splitting in an Al-InAs nanowire topological superconductor as a signature of majorana fermions,” *Nature Physics* **8**, 887–895 (2012).
- [89] H. O. H. Churchill, V. Fatemi, K. Grove-Rasmussen, M. T. Deng, P. Caroff, H. Q. Xu, and C. M. Marcus, “Superconductor-nanowire devices from tunneling to the multichannel regime: Zero-bias oscillations and magnetoconductance crossover,” *Phys. Rev. B* **87**, 241401 (2013).
- [90] A. D. K. Finck, D. J. Van Harlingen, P. K. Mohseni, K. Jung, and X. Li, “Anomalous modulation of a zero-bias peak in a hybrid nanowire-superconductor device,” *Phys. Rev. Lett.* **110**, 126406 (2013).
- [91] J. Liu, A. C. Potter, K. T. Law, and P. A. Lee, “Zero-bias peaks in the tunneling conductance of spin-orbit-coupled superconducting wires with and without majorana end-states,” *Phys. Rev. Lett.* **109**, 267002 (2012).
- [92] M. T. Deng, C. L. Yu, G. Y. Huang, M. Larsson, P. Caroff, and H. Q. Xu, “Anomalous zero-bias conductance peak in a nb-insb nanowire-nb hybrid device,” *Nano Letters* **12**, 6414–6419 (2012).
- [93] C. Nayak, S. H. Simon, A. Stern, M. Freedman, and S. D. Sarma, “Non-abelian anyons and topological quantum computation,” *Rev. Mod. Phys.* **80**, 1083 (2008).
- [94] S. Das Sarma, M. Freedman, and C. Nayak, “Topologically protected qubits from a possible non-abelian fractional quantum hall state,” *Physical Review Letters* **94**, 166802 (2005).
- [95] Y. Li, A. Kundu, F. Zhong, and B. Seradjeh, “Tunable floquet majorana fermions in driven coupled quantum dots,” *Phys. Rev. B* **90**, 121401 (2014).
- [96] F. Medina-Cuy, D. Martínez, F. Domínguez-Adame, and P. A. Orellana, “Majorana bound states in a driven quantum dot,” *The European Physical Journal Plus* **138**, 701 (2023).
- [97] J. Cayssol, B. Dóra, F. Simon, and R. Moessner, “Floquet topological insulators,” *Phys. Status Solidi RRL* **7**, 101–108 (2013).
- [98] M. S. Rudner, N. H. Lindner, E. Berg, and M. Levin, “Anomalous edge states and the bulk-edge correspondence for periodically driven two-dimensional systems,” *Phys. Rev. X* **3**, 031005 (2013).
- [99] A. Gómez-León and G. Platero, “Floquet-bloch theory and topology in periodically driven lattices,” *Phys. Rev. Lett.* **110**, 200403 (2013).
- [100] M. S. Rudner and N. H. Lindner, “Band structure engineering and non-equilibrium dynamics in floquet topological insulators,” *Nature Reviews Physics* **2**, 229–244 (2020).
- [101] Y. Oreg, G. Refael, and F. von Oppen, “Helical liquids and majorana bound states in quantum wires,” *Phys. Rev. Lett.* **105**, 177002 (2010).
- [102] J. Alicea, “Majorana fermions in a tunable semiconductor device,” *Phys. Rev. B* **81**, 125318 (2010).
- [103] L.-J. Lang and S. Chen, “Majorana fermions in density-modulated p -wave superconducting wires,” *Phys. Rev. B* **86**, 205135 (2012).
- [104] M. Z. Hasan and C. L. Kane, “Colloquium: Topological insulators,” *Rev. Mod. Phys.* **82**, 3045 (2010).
- [105] S. Fölsch, J. Martínez-Blanco, J. Yang, K. Kanisawa, and S. C. Erwin, “Quantum dots with single-atom precision,” *Nature Nanotechnology* **7** (2014), 10.1038/nnano.2014.129.
- [106] J. B. Miller, D. M. Zumbühl, C. M. Marcus, Y. B. Lyanda-Geller, D. Goldhaber-Gordon, K. Campman, and A. C. Gossard, “Gate-controlled spin-orbit quantum interference effects in lateral transport,” *Phys. Rev. Lett.* **90**, 076807 (2003).
- [107] Q.-f. Sun, J. Wang, and T.-h. Lin, “Control of the supercurrent in a mesoscopic four-terminal josephson junction,” *Phys. Rev. B* **62**, 648–660 (2000).
- [108] B. Pal, A. Chakraborty, P. K. Sivakumar, M. Davydova, A. K. Gopi, A. K. Pandeya, J. A. Krieger, Y. Zhang, M. Date, S. Ju, N. Yuan, N. B. M. Schröter, L. Fu, and S. S. P. Parkin, “Josephson diode effect from cooper pair momentum in a topological semimetal,” *Nature Physics* **18**, 1228–1233 (2022).
- [109] P. Hosur and D. Palacios, “Proximity-induced equilibrium supercurrent and perfect superconducting diode effect due to band asymmetry,” *Phys. Rev. B* **108**, 094513 (2023).
- [110] P. San-Jose, E. Prada, and R. Aguado, “Mapping the topological phase diagram of multiband semiconductors with supercurrents,” *Physical Review Letters* **112**, 137001 (2014).
- [111] J. Cayao and A. M. Black-Schaffer, “Finite length effect on supercurrents between trivial and topological superconductors,” *The European Physical Journal Special Topics* **227**, 1387–1396 (2018).
- [112] B. D. Josephson, “The discovery of tunnelling supercurrents,” *Rev. Mod. Phys.* **46**, 251–254 (1974).
- [113] J. A. van Dam, Y. V. Nazarov, E. P. A. M. Bakkers, S. De Franceschi, and L. P. Kouwenhoven, “Supercurrent reversal in quantum dots,” *Nature* , 667–670 (2006).
- [114] P. Jarillo-Herrero, J. A. van Dam, and L. P. Kouwenhoven, “Quantum supercurrent transistors in carbon nanotubes,” *Nature* **439**, 953–956 (2006).
- [115] V. Mourik, K. Zuo, S. M. Frolov, S. R. Plissard, E. P. A. M. Bakkers, and L. P. Kouwenhoven, “Signatures of majorana fermions in hybrid superconductor-semiconductor nanowire devices,” *Science* **336**, 1003–1007 (2012).
- [116] S. Nadj-Perge, I. K. Drozdov, J. Li, H. Chen, S. Jeon, J. Seo, A. H. MacDonald, B. A. Bernevig, and A. Yazdani, “Observation of majorana fermions in ferromagnetic atomic chains on a superconductor,” *Science* **346**, 602–607 (2014).
- [117] T. Dvir, G. Wang, N. van Loo, C.-X. Liu, G. P. Mazur, A. Bordin, S. L. D. ten Haaf, J.-Y. Wang, D. van Driel,

- F. Zatelli, X. Li, F. K. Malinowski, S. Gazibegovic, G. Badawy, E. P. A. M. Bakkers, M. Wimmer, and L. P. Kouwenhoven, "Realization of a minimal kitaev chain in coupled quantum dots," *Nature* **614** (2023), [10.1038/s41586-022-05585-1](https://doi.org/10.1038/s41586-022-05585-1).
- [118] W. Samuelson, V. Svensson, and M. Leijnse, "Minimal quantum dot based kitaev chain with only local superconducting proximity effect," *Phys. Rev. B* **109**, 035415 (2024).
- [119] D. M. Eigler and E. K. Schweizer, "Positioning single atoms with a scanning tunnelling microscope," *Nature* **344** (1990), [10.1038/344524a0](https://doi.org/10.1038/344524a0).
- [120] H. Kim, A. Palacio-Morales, T. Posske, L. Rózsa, K. Palotás, L. Szunyogh, M. Thorwart, and R. Wiesendanger, "Toward tailoring majorana bound states in artificially constructed magnetic atom chains on elemental superconductors," *Science Advances* **4**, eaar5251 (2018).
- [121] L. Schneider, K. T. Ton, I. Ioannidis, J. Neuhaus-Steinmetz, T. Posske, R. Wiesendanger, and J. Wiebe, "Proximity superconductivity in atom-by-atom crafted quantum dots," *Nature* **621** (2023), [10.1038/s41586-023-06312-0](https://doi.org/10.1038/s41586-023-06312-0).
- [122] J. Gabelli and B. Reulet, "Shaping a time-dependent excitation to minimize the shot noise in a tunnel junction," *Phys. Rev. B* **87**, 075403 (2013).
- [123] Q. Cheng, Y. Pan, H. Wang, C. Zhang, D. Yu, A. Gover, H. Zhang, T. Li, L. Zhou, and S. Zhu, "Observation of anomalous π modes in photonic floquet engineering," *Phys. Rev. Lett.* **122**, 173901 (2019).
- [124] S. Ryu, A. P. Schnyder, A. Furusaki, and A. W. W. Ludwig, "Topological insulators and superconductors: tenfold way and dimensional hierarchy," *New Journal of Physics* **12**, 065010 (2010).